University of Central Lancashire
UCLan

Central Lancashire Online Knowledge (CLoK)

Title	Dynamic Temperature–Vacuum Swing Adsorption for Sustainable Direct Air Capture: Parametric Optimisation for High-Purity CO_2 Removal
Type	Article
URL	https://clok.uclan.ac.uk/id/eprint/56314/
DOI	
Date	2025
Citation	Nasiri-Ghiri, Maryam, Nasriani, Hamid Reza, Khajenoori, Leila, Mohammadkhani, Samira and Williams, Karl S (2025) Dynamic Temperature–Vacuum Swing Adsorption for Sustainable Direct Air Capture: Parametric Optimisation for High-Purity CO_2 Removal. Sustainability.
Creators	Nasiri-Ghiri, Maryam, Nasriani, Hamid Reza, Khajenoori, Leila, Mohammadkhani, Samira and Williams, Karl S

It is advisable to refer to the publisher's version if you intend to cite from the work.

For information about Research at UCLan please go to http://www.uclan.ac.uk/research/

All outputs in CLoK are protected by Intellectual Property Rights law, including Copyright law. Copyright, IPR and Moral Rights for the works on this site are retained by the individual authors and/or other copyright owners. Terms and conditions for use of this material are defined in the http://clok.uclan.ac.uk/policies/

sustainability

MDPI

Article

Dynamic Temperature–Vacuum Swing Adsorption for Sustainable Direct Air Capture: Parametric Optimisation for High-Purity CO_2 Removal

Maryam Nasiri-ghiri [1], Hamid Reza Nasriani*[1], Leila Khajenoori[1], Samira Mohammadkhani[2] and Karl S Williams[1]

[1,] School of Engineering & Computing, University of Central Lancashire, Preston PR1 2HE, UK
[2] Geological Survey of Denmark and Greenland, Department of Geo-energy and Storage, ΦsterVoldgade 10, 1350 Copenhagen, Denmark
* hrnasriani@uclan.ac.uk

Abstract: Direct Air Capture (DAC), as a complementary strategy to Carbon Capture and Storage (CCS), offers a scalable and sustainable pathway to remove CO_2 directly from the ambient air. This study presents a detailed evaluation of the amine-functionalised metal-organic framework (MOF) sorbent, mmen-Mg_2(dobpdc), for DAC using a Temperature Vacuum Swing Adsorption (TVSA) process. While this sorbent has demonstrated promising performance in point-source CO_2 capture, this is the first dynamic simulation-based study to rigorously assess its effectiveness for low-concentration atmospheric CO_2 removal. A transient one-dimensional TVSA model was developed in Aspen Adsorption and validated against experimental breakthrough data to ensure accuracy in capturing both the sharp and gradual adsorption kinetics. To enhance process efficiency and sustainability, this work provides a comprehensive parametric analysis of key operational factors, including air flow rate, temperature, adsorption/desorption durations, vacuum pressure, and heat-exchanger temperature, on process performance, including CO_2 purity, recovery, productivity, and specific energy consumption. Under optimal conditions for this sorbent (vacuum pressure lower than 0.15 bar and feed temperature below 15 ^{0}C) the TVSA process achieved ~98% CO_2 purity, recovery over 70% and specific energy consumption about 3.5 MJ/KgCO_2. These findings demonstrate that mmen-Mg_2(dobpdc) can achieve performance comparable to benchmark DAC sorbents in terms of CO_2 purity and recovery, underscoring its potential for scalable DAC applications. This work advances the development of energy efficient carbon removal technologies and highlight the value of step-shape isotherm adsorbents in supporting global carbon-neutrality goals.

Keywords: Carbon Dioxide; Adsorption; Simulation; Sustainability, Sensitivity; TVSA; Metal Organic Frameworks, Amine-functionalised MOFs

Academic Editor: Firstname Lastname

Received: date
Revised: date
Accepted: date
Published: date

Citation: To be added by editorial staff during production.

Copyright: © 2025 by the authors. Submitted for possible open access publication under the terms and conditions of the Creative Commons Attribution (CC BY) license (https://creativecommons.org/licenses/by/4.0/).

1. Introduction

The continued rise in atmospheric CO_2—driven by population growth, urbanisation, and industrialisation—has intensified global climate change, making carbon mitigation a critical priority for long-term environmental sustainability . Despite growing efforts to decarbonise, fossil fuels such as coal, oil, and natural gas remain the dominant energy sources, and account for over 75% of anthropogenic CO_2 emissions [1-5]. While renewable

energy technologies (e.g., wind, solar, hydro, and bioenergy) offer low-carbon alternatives, their adoption is challenged by intermittency, storage limitations, and spatial constraints [6-11]. While the global energy transition is underway, the pace of decarbonisation remains insufficient to meet the targets set by the Paris Agreement and ensure climate sustainability. Atmospheric CO_2 levels have risen from approximately 180 parts per million (ppm) during the last three glacial cycles to about 426 ppm as of May 2024, with an ongoing annual increase of around 2 ppm [12,13]. To limit global temperature, rise to below 2 ^{0}C, with an aspirational target of 1.5 ^{0}C above pre-industrial levels, as outlined in Paris Agreement- large scale removal of atmospheric CO_2 is required, with estimates indicating a need to extract 10 GtCO_2/year by 2050, increasing to 20 GTCO_2/year thereafter [14,15].

Direct air capture (DAC) has emerged as a promising negative emission technology to address both current and historical CO_2 emissions, complementing traditional carbon capture, utilisation, and storage (CCUS) technologies that primarily target point sources [7,16]. Among the available DAC technologies, absorption using liquid solvents is the most widely applied due to its high CO_2 capacity and relatively low cost. However, its application in DAC is limited by challenges such as complex waste management, solvent degradation, evaporation losses, and high thermal energy demand for regeneration, especially under variable atmospheric conditions [17-19] . While alternatives like ionic liquids offer improved thermal stability, their practical use is constrained by thermal decomposition and high cost [20-23]. These limitations have shifted attention toward adsorption-based DAC processes, which offer the advantage of partially overcoming the limitations associated with absorption [24].

Various porous materials, including carbon, zeolites, silica, resin, and metal-organic frameworks (MOFs), have been investigated for CO_2 separation [25-31]. While activated carbons (ACs) and zeolites have been widely studied for DAC due to their porosity and thermal stability, both exhibit significant limitations under ambient conditions. ACs exhibit reduced CO_2 capacity under humid environments and may degrade thermally during repeated regeneration, particularly at high desorption temperatures [32-33], though modification such as hydrophobic surface treatments and potassium carbonate incorporation offer partial improvements [34-36]. Zeolites offer high CO_2 selectivity and strong structural stability but suffer from moisture sensitivity and loss adsorption capacity above 100 °C, requiring high regeneration energy [37-39]. To overcome these issues, approaches such as core–shell hydrophobic coatings and ion exchange have been investigated, with Fe-modified 13X zeolites showing enhanced performance [21]. Recent advances have positioned MOFs as promising candidates, offering extremely high surface areas (up to 7,140 m^2/g, and theoretically even 10,000 m^2/g) and structural tunability through metal-organic coordination, with over 88,000 MOF structures reported and many more possible [40,41]. The mechanisms and strategies for optimising CO_2 capture in MOFs under high concentration conditions are well established, resulting in the development of highly stable and high-performing materials that are now commercialised for industrial use. For example, CALF-20, a MOF developed for flue gas CO_2 capture, features channel-like pores of approximately ~3 Å and demonstrated a CO_2 uptake of 4.07 mmol g^{-1} at 293 K and 1.2 bar, with an IAST selectivity of 230 for a 10/90 CO_2/N_2 mixture [42]. Similarly, UTSA-16, an ultra-microporous MOF based on citric acid, achieves a CO_2 uptake of 4.25 mmol g^{-1} with pore dimensions of 3.3 × 5.4 $^0A^2$ [43]. Moreover, recent developments in MOF design have explored the integration of catalytic sites for simultaneous CO_2 capture and conversion, broadening the potential application of these materials beyond pure adsorption processes [44,45]. However, for capturing CO_2 directly from the air, with its extremely low partial pressure, these MOFs like CALF-20 and UTSA-16, often underperform due to weak binding sites [42,43] and moisture-induced degradation [46].

Nomenclature

R_p	Particle radius (m)	K_{fk}	Film resistance coefficient (m/s)
R_b	Bed radius (m)	K_{pk}	Macropore diffusion coefficient (m^2/s)
a_P	External surface area per unit volume of the particle [1/m]	K_k	Overall mass transfer coefficient (1/s)
q	Feed flow rate (Kmol/h)	D_{kk}	Knudsen diffusion coefficient (m^2/s)
ΔH_{CO2}	CO_2 heat of adsorption (KJ/mol)	V_g	Superficial gas velocity (m/s)
ΔH_{N2}	N_2 heat of adsorption (KJ/mol)	P_{feed}	Feed pressure (bar)
C_{ps}	Crystal heat capacity (KJ/Kmol.K)	$F_{product}$	Product flow rate (Kmol/h)
K	Thermal conductivity(W/m.K)	F_{feed}	Feed flow rate (Kmol/h)
HTC	Heat transfer coefficient [$W/m^2.K$]	k_A	Avrami rate constant (1/s)
a_{Hx}	Heat exchanger surface area per unit volume (1/m)	n_A	Avrami fractional constant
Q_{Hx}	Heat supplied or removed by the heat exchanger (W/m^3)	T cycle	Full cycle time (s)
ΔH	Isosteric heat of adsorption (KJ/mol)	$W_{adsorbent}$	Adsorbent mass (Kg)
C_p	Heat capacity at constant pressure (KJ/mol.K)	P_{vac}	Vacuum pressure (bar)
C_v	Heat capacity at constant volume (KJ/mol.K)	y	Gas mole fraction
C_{ps}	Specific solid phase heat capacity (MJ/Kmol·K)	AARD	Average absolute relative deviation
C_{vg}	Specific gas phase heat capacity (MJ/kmol·K),	RMSE	Root mean squared error
P_{step}	Isotherm step pressure (bar)	**Greek letters**	
q^*_1	CO_2 uptake before P_{step} (mol/Kg)	ρ_g	gas density (Kg/m^3)
q^*_2	CO_2 uptake after P_{step} (mol/Kg)	ρ_s	Solid (crystal) density(Kg/m^3)
q_L	Low-affinity adsorption capacity (mol/Kg)	γ	Isotherm parameters (sharpness of the transition)
q_H	High-affinity adsorption capacity (mol/Kg)	λ	Isotherm parameter controlling the effect of temperature(1/K)
q_U	Ultimate affinity adsorption capacity(mol/Kg)	μ	Fluid viscosity ($N.s/m^2$)
n	Surface homogeneity factor	ε_p	intraparticle void fraction ($m^3_{void}/m^3_{particle}$)
R	Gas constant (J/mol. K)	ε_b	Bed porosity (m^3_{void}/m^3_{bed})
b	Longmuir constant (isotherm parameters) (1/bar)	ε_t	Total bed porosity ($m^3_{void}+m^3_{pore}$)/ m^3_{bed}
W	Solid loading (Kmol/Kg)	γ	Specific heat ratio
W*	Equilibrium solid loading (Kmol/Kg)	η	Pump efficiency
Sh_k	Sherwood number	ω	Isotherm parameter (smooth transition function)
Re	Reynolds number	**Abbreviations**	
Sc_k	Schmidt number	DAC	Direct Air Capture
MTC	Mass transfer coefficient (1/s)	MOF	Metal Organic Framework
LDF	Linear driving force	CCUS	carbon capture, utilisation, and storage
		TVSA	Temperature vacuum swing adsorption

For low-concentration CO_2 capture, chemisorption is advantageous by providing strong binding affinity. In particular, amine-functionalisation of porous materials via physical impregnation, chemical grafting, or in situ polymerisation has proven effective in improving both CO_2 capture capacity and selectivity [14,47,48]. This approach has been

particularly successful with MOFs, enabling the design of highly tuneable materials (via linker or metal–ligand modifications) and superior CO_2 selectivity and capacity through strong Lewis base sites [49,50]. A prominent example is mmen-Mg_2(dobpdc), developed by grafting N, N′ dimethyl ethylene diamine (mmen) and ethylene diamine (ED) onto the Mg_2(dobpdc) framework [25]. This sorbent exhibits exceptional CO_2 capacity at low pressures (2.0 mmol/g (8.1 wt %) at 0.39 mbar and 25 ^{0}C) and benefits from fast adsorption kinetics and cooperative adsorption mechanisms that enhance efficiency [51]. In addition, mmen-Mg_2(dobpdc) demonstrated favourable recyclability and thermal stability. McDonald et al.[49] reported consistent performance over multiple adsorption–desorption cycles, while later research confirmed structural integrity during vacuum or N_2-based regeneration up to 150 ^{0}C and its tolerance to moderate humidity [52]. These characteristics further reinforce its suitability for long-term DAC operation. Subsequent studies have confirmed its potential under DAC conditions [38,50,53-55] . However, Darunte et al. [56] evaluated its performance for CO_2 capture from ultra-dilute feeds and observed reduced CO_2 capture fraction due to the unique stepped isotherm and kinetic characteristics of this sorbent, Further investigation under 1000 ppm CO_2 confirmed the high working capacity of mmen-Mg_2(dobpdc) despite mass transfer limitations [57].

To maximise DAC efficiency, the choice of regeneration strategy has a critical role in determining overall process efficiency. TVSA has been identified as the most suitable regeneration strategy for amine-functionalised solid sorbents, offering high working capacities and lower energy demands without requiring extreme vacuum or temperature [58-60] , which makes it well suited for DAC, where careful balance between sorbent efficiency and the regeneration energy demand is essential. Phase-change adsorbents like mmen-Mg_2(dobpdc), which exhibit sharp stepwise isotherm transitions, particularly benefit from TVSA because it enables effective regeneration with minimal energy input [51].

While several studies have explored the application of different amine-functionalised MOFs for CO_2 capture from flue gas [61-62], and indoor environment[57], this study specifically targets the 400 ppm CO_2 concentration typical of DAC, where lower partial pressures intensify both kinetic and thermodynamic challenges. A dynamic simulation of a modular DAC process is developed using the amine-functionalised MOF, mmen-Mg_2(dobpdc), known for its distinctive step-shaped CO_2 adsorption isotherm. A one-dimensional TVSA framework, implemented in Aspen Adsorption, incorporates mass, energy, and momentum balances to simulate the transient behaviour of adsorption–desorption cycles at lab scale. Sensitivity analysis is conducted to evaluate the effects of key operating parameters—feed flow rate and temperature, vacuum pressure, and step durations—on critical performance metrics, including CO_2 purity, recovery, productivity, and specific energy consumption. The findings establish operational guidelines to improve process efficiency and provide valuable insights for the design and optimisation of energy-efficient MOF based DAC systems, aligning with broader environmental sustainability goals.

2. Materials and Methods

During adsorption, CO_2 is captured by high-affinity porous material, followed by a regeneration step that release CO_2 and restore the sorbent's capacity. The efficiency of this process depends on the sorbent properties, operating conditions, and regeneration strategy. In this study, a TVSA process is simulated in an axial-flow fixed bed reactor, where mmen-Mg_2(dobpdc) is used as the adsorbent. TVSA combines mild heating and vacuum pressure reduction to desorb CO_2 while restoring the sorbent's adsorption capacity for subsequent cycles [63]. The released CO_2 is collected through a condenser to ensure high purity, while a heat exchanger is integrated within the bed to optimise thermal management during adsorption and desorption.

2.1. Simulation Framework (Numerical Modelling and Assumption)

A dynamic model for non-isothermal, adiabatic TVSA is developed in Aspen Adsorption to evaluate the technical performance of mmem-Mg_2(dobpdc) under DAC conditions. The software simulates the complete adsorption/desorption cycle, incorporating mass, energy, and momentum balances to predict system behaviour and evaluate process parameters. To solve the coupled partial differential equations (PDEs) under specified boundary conditions, this study applies a set of assumptions to simplify the computational complexity while maintaining model accuracy as follows:

- The sorbent has a spherical shape with uniform, continuous properties, as the selected particles used in the experimental studies were derived from MOF powders composed of fine crystallites that were agglomerated and sieved to obtain particles with controlled and consistent size [56].
- The gas phase follows ideal gas behaviour, which is a reasonable approximation under the low operating pressures and dilute CO_2 concentrations typical of DAC systems.
- Constant adsorbed phase heat capacity is assumed because the amount of adsorbed CO_2 is small in DAC.
- The column thickness effect is ignored, assuming the adiabatic conditions.
- No parasitic reactions between the gas and the adsorbent.
- A one-dimensional model incorporating convection.
- The air flow mixture consists of CO_2 and N_2, with CO_2 as the sole adsorbed component.
- CO_2 adsorption kinetics differ below and above P_{step}; the model captures this through dual-regime rate constants derived from experimental fitting [56].

Thes assumptions are consistent with prior TVSA modelling studies [53,54,64,65], allowing focus on parametric influences rather than complex 2D effects or humidity interactions.

The exceptional CO_2 selectivity of mmen-Mg_2(dobpdc) allows the exclusion of N_2 and O_2 from adsorption considerations. McDonald [49] reported that CO_2/N_2 selectivity of this sorbent exceed 49000, with negligible uptake of O_2 and N_2. Mason et al. [66] further confirmed that, N_2 adsorption was undetectable in mixed-gas conditions. Based on these findings, N_2 and O_2 can be treated as inert gases in this model. Additionally, the effect of water adsorption is not considered in the present study, as experimental results have consistently demonstrated that the presence of H_2O has minimal influence on CO_2 adsorption in mmen-Mg_2(dobpdc). Notably, CO_2 uptake under humid conditions is comparable to, or slightly higher than, that observed in dry environments [49-66]. Similarly, breakthrough experiments conducted at 50% relative humidity under DAC conditions illustrated an increase in CO_2 capture capacity from 2.16 mmol/gr to 2.41 mmol/gr [67].

2.1.1. Packed Bed Specification

The packed-bed reactor is designed based on the experimental parameters reported by Darunte. [56]. The air feed conditions are set at 1.1013 bar and 25 ^{0}C, with a molar composition of 99.96% N_2 and 0.04% CO_2. Table 1 lists the key design parameters for the packed bed reactor model used in this study. These parameters define the physical characteristics of the adsorption column and operating conditions, which govern adsorption behaviour and system performance by influencing flow dynamics, mass transfer, and adsorbent capacity.

Table 1. Design and operating parameters of the Packed bed used for simulation [56].

Parameters	Unit	Values
Bed Length	m	0.055
Bed Internal Radius	m	0.004
Desorption Temperature	^{0}C	115
Adsorption Temperature	^{0}C	23
Particle Radius	m	2.25e-4
Crystal Density	Kg/m^3	860
Bed Porosity	fraction	0.32
Adsorbent Weight	g	60
Particle Porosity	fraction	0.85
Feed Flow rate	N ml/min	17.2

2.1.2. Adsorption Equilibrium and Kinetics

The development of the model requires accurate adsorption characteristics. The relevant thermal properties used in the simulation are summarised in Table 2.

Table 2. Thermal characteristics of mmen-Mg$_2$(dobpdc) and adsorbates.

Parameters	Unit	Values	Reference
CO_2 heat of adsorption	KJ/mol	-71	[68]
N_2 heat of adsorption	KJ/mol	-18	[57]
Heat capacity of the crystal	KJ/Kg.K	1.6	[51]
CO_2 heat capacity	KJ/Kmol.K	37.4673	(Aspen Plus)
N_2 heat capacity	KJ/Kmol.K	29.1806	(Aspen Plus)
Thermal conductivity	W/m.K	0.3	[69]

The adsorption behaviour of mmen-Mg$_2$(dobpdc) follows step-shape (S-shape) CO_2 adsorption isotherm, characterised by two distinct adsorption regimes. Below isotherm transition pressure (P_{step}), CO_2 adsorption occurs through the reaction of two free amine groups with CO_2, forming ammonium carbamate, similar to conventional amine functionalised sorbents. Above P_{step}, the cooperative adsorption mechanism is observed, where both ends of the diamine participate in CO_2 binding, leading to the formation of one-dimensional ammonium carbamate chains aligned along the Mg^{2+} framework [51]. This study employs the model proposed by Darunte [56], which builds upon Hefti's framework [54], incorporating the Sips isotherm to accurately describe CO_2 adsorption below P_{step} as defined by equations 1 - 8. q_1^* and q_2^* describe CO_2 uptake before and after P_{step} respectively, w presents a smooth transition function between two regions. q_L, q_H, and q_U represent the affinity of sorbents, and n reflects the surface homogeneity factor. The temperature dependence of P_{step} is calculated by equation 8 where $p_{step,0}$ = 0.8 mbar at T_0 = 313.5 ^{0}K and ΔH_{step} represent the enthalpy change associated with the adsorption transition [51]. Darunte [56], fitted the isotherm model to the experimental data to determine the isotherm parameters. The fitted parameters with the formula of temperature-dependent parameters are presented in Table 3.

$$q_{total} = q_1^* + q_2^* \quad (1)$$

$$q_1^* = q_{low} \times (1 - w) + q_{sat} \times w \quad (2)$$

$$q_2^* = (q_{high} - q_{sat}) \times w \quad (3)$$

$$q_{low} = \frac{q_L (b_L p)^{n_L}}{1 + (b_L p)^{n_L}} \quad (4)$$

$$q_{high} = \frac{q_H b_H p}{1 + b_H p} + q_U p \qquad p < p_{step} \quad (5)$$

$$q_{sat} = \frac{q_L (b_L p_{step})^n}{1 + (b_L p_{step})^n} \qquad p > p_{step} \quad (6)$$

$$w = \left[\frac{\exp\left(\frac{\log(p) - \log(p_{step})}{\sigma}\right)}{1 + \exp\left(\frac{\log(p) - \log(p_{step})}{\sigma}\right)}\right]^{\gamma} \quad (7)$$

$$p_{step}(T) = p_{step,0} \exp\left[-\frac{\Delta H_{step}}{R}\left(\frac{1}{T_0} - \frac{1}{T}\right)\right] \quad (8)$$

Table 3. Isotherm fitting parameters and equations for temperature-dependent variables [56].

Parameter	Unit	Value	Parameters	Unit	Values
q_L	mol/Kg	28.25	ΔH_{step}	KJ/mol	-62.49
b_{L0}	1/bar	2.51e-15	ΔH_L	KJ/mol	70.74
n_0	-	0.518	ΔH_n	KJ/mol	1.35
q_H	mol/Kg	3.46	ΔH_H	KJ/mol	67.72
b_{H0}	1/bar	2.42e-11	ΔH_u	KJ/mol	18.67
q_{u0}	mol/Kg.bar	5.27e-4	λ_1	-	1.74e-2
Υ	-	4	λ_2	$1/^0K$	6.53

Temperature- dependent variables formula

$$b_U = b_{L0} \exp\left(\frac{\Delta H_L}{RT_g}\right) \qquad q_U = q_{u0} \exp\left(\frac{\Delta H_u}{RT_g}\right)$$

$$\sigma = \lambda_1 \exp\left[\lambda_2\left(\frac{1}{T_0} - \frac{1}{T_g}\right)\right] \qquad b_H = b_{H0} \exp\left(\frac{\Delta H_H}{RT_g}\right)$$

$$n = n_0 \exp\left(\frac{\Delta H_{Ln}}{RT_g}\right)$$

The parameters b_L and b_H represent the temperature-dependent adsorption equilibrium constants for the low-affinity (L) and high-affinity (H) sites, respectively. The terms ΔH_L and ΔH_H denote the heat of adsorption for low- and high-affinity sites, respectively, while ΔH_u corresponds to the heat of adsorption for uniform adsorption sites. The parameter σ characterises the sharpness of the phase transition in the cooperative adsorption mechanism. To describe the adsorption kinetic ($\frac{\partial W_i}{\partial t}$), a dual-kinetic approach based on the work of Darunte et al.[56] was adopted. Their study demonstrated the conventional linear driving force (LDF) model alone could not adequately capture the experimental kinetic data. Consequently, they proposed two different kinetic models based on CO_2 partial pressure: an LDF model for pressure below the step pressure (P_{step}), where CO_2 adsorption proceeds via ammonium carbamate formation with a 2:1 amine-to-CO_2 stoichiometry [51,70] (Equation 9), and an Avrami fractional-order model for pressures above P_{step}. At these higher pressures, CO_2 adsorption is governed by cooperative

insertion, characterised by a rapid saturation of amine sites due to a 1:1 stoichiometry and chain propagation effects (Equation 10)[56].

$$\frac{\partial W_i}{\partial t} = K_k(w^*{}_i - w_i) \qquad \text{p} < \text{Pstep} \tag{9}$$

$$\frac{\partial W_i}{\partial t} = K_A^{n_A} t^{n_A - 1}(w^*{}_i - w_i) \qquad \text{p} > \text{Pstep} \tag{10}$$

In Equation 9, the initial value of the overall mass transfer coefficient K_k (1/s) is estimated using a lumped resistance model, as expressed in Equation 11, which accounts for both external film resistance and macropore diffusion [71]. Since such correlations alone are often insufficiently precise, the initial estimate is subsequently refined by calibrating the simulation results against experimental observations.

$$\frac{1}{K_k} = \frac{r_p}{3K_{fk}} + \frac{r_p^2}{15\,\varepsilon_p K_{pk}} \tag{11}$$

In Equation 11, r_p and ε_p represent particle radius (m) and intraparticle void fraction, respectively. The film resistance coefficient K_{fk}(m/s) is calculated using Equation 12-15. The K_{pk} is the macropore diffusion coefficient (m²/s) which is calculated by Equation 16-17.

$$K_{fk} = sh_k \frac{D_{mk}}{2r_p} \tag{12}$$

$$sh_k = 2 + 1.1 \times Sc_k^{1/3} Re^{0.6} \tag{13}$$

$$Sc_k = \frac{\mu}{D_{mk}\rho_g} \tag{14}$$

$$Re = \frac{v_g 2 r_p \rho_g}{\mu} \tag{15}$$

$$\frac{1}{K_{pk}} = \tau\left(\frac{1}{D_{Kk}} + \frac{1}{D_{mk}}\right) \tag{16}$$

$$D_{Kk} = 97 r_p \left(\frac{T}{M_k}\right)^{0.5} \tag{17}$$

The Sherwood (sh_k), Reynolds (Re), and Schmidt numbers (Sc_k) are defined in Equations 12-15. The Knudsen diffusion coefficient D_{Kk} (m²/s), shown in Equation 17, is a function of temperature (⁰K), molar mass M_k (g/mol), and pore radius. The total molecular diffusion (D_{mk}) is estimated using data from the Aspen Properties database.

In Equation 10, the Avrami parameters k_A, t, $w^*{}_i$, and n_A represent the Avrami rate constant, time, saturation capacity, and Avrami fractional constant, respectively. The constant parameters (K_A) and (n_A) were fitted to experimental data, with values of 4.36e-5 (1/s) and 1.5 for 0.4 mbar CO_2 partial pressure [56].

2.1.3. Energy Balance

In a non-isothermal system, Energy balance applies to both gas and solid phases. The energy balance for the solid phase is expressed as Equation 18. This equation includes a contribution from heat transfer through convection, the heat released during adsorption,

the heat capacity of the adsorbed phase, and the heat transfer between the gas and solid phase. The gas phase energy balance accounts for the effects of convection, heat accumulation, heat transfer between the gas and solid phases, and the heat of reaction, which are outlined in Equation 19. The adsorbed-phase heat capacity and heat transfer coefficient are estimated by using Aspen software.

$$\rho_s C_{ps} \frac{\partial T_s}{\partial t} + \sum H_k + \rho_s \sum (\Delta H_k \frac{\partial w_k}{\partial t}) - HTC a_p (T_g - T_s) = 0 \quad (18)$$

With ρ_s denotes solid phase density (Kg/m^3), C_{ps} is Specific heat capacity of the solid phase (MJ/Kmol·K), T_g and T_s represent the temperatures of solid and gas phase (K), H_k is the heat of adsorption for component K (J/Kg), HTC refer to the heat transfer coefficient between the gas and solid [W/m^2.K], and a_p is the external surface area per unit volume of the particle [1/m].

$$C_{vg} v_g \rho_g \frac{\partial T_g}{\partial z} + \varepsilon_t C_{vg} \rho_g \frac{\partial T_g}{\partial t} + HTC\ a_p (T_g - T_s) + a_{Hx} Q_{Hx} = 0 \quad (19)$$

In this equation, C_{vg} represents the specific heat capacity of the gas phase (MJ/kmol·K), v_g is the superficial gas velocity (m/s), ρ_g is gas density (Kg/m^3), ε_t denotes the total bed porosity. Additionally, a_{Hx} is the heat exchanger surface area per unit volume (1/m), and Q_{Hx} refers to the heat supplied or removed by the heat exchanger (W/m^3).

2.1.4. Pressure Drop

Since the system operates at a constant mass flow rate with uniform adsorbent distribution, steady-state conditions are assumed for pressure drop across the bed. Consequently, The Ergun equation (Equation 20) is applied to describe the total pressure drop, accounting for both viscous and kinetic energy loss in the fixed bed. In this equation, $\boldsymbol{\mu_g}$ refers to gas viscosity (N.s/m^2), u_g is the superficial velocity of the gas phase (m/s) , r_p represents the particle radius (m), ε is the interparticle voidage fraction ($m^3_{(Void)}/m^3_{(Bed)}$), and ρ_g is the gas phase density (Kg/m^3).

$$-\frac{\partial P_{total}}{\partial z} = 150 \frac{\mu_g (1-\varepsilon)^2}{\varepsilon^3 (2r_p)^2} u_g + 1.75 \frac{(1-\varepsilon)\rho_g}{2 r_p \varepsilon^3} u_g^2 \quad (20)$$

2.2. Process Design: Basis and Criteria

A cyclic adsorption model was developed as the basis for evaluating mmem-Mg$_2$(dobpdc) under DAC conditions. The process flowchart diagram is depicted in Figure 1. The TVSA sequences were defined in five sequential steps, as outlined below:

- Adsorption: Ambient air flows through the packed bed, where CO_2 is selectivity adsorbed onto the sorbent while CO_2-depleted air is released.
- Evacuation: The system pressure is reduced to remove N_2.
- Heating + Evacuation: The bed is heated using a heat exchanger to reach the regeneration temperature while maintaining vacuum conditions to promote efficient CO_2 desorption.
- Cooling: The heat exchanger cools the bed to maintain thermal stability, prevent amine degradation, and facilitate the next adsorption step.

- Pressurisation: The system is returned to atmospheric pressure by gradually reintroducing air, initiating the next adsorption cycle.

The initial process cycle duration, considering the breakthrough behaviour, is detailed in Table 4. An event-driven approach was applied to the cooling and pressurisation step to eliminate unnecessary idle time and improve overall cycle efficiency.

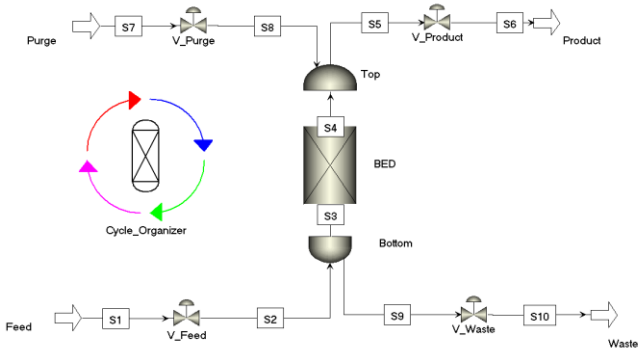

Figure 1. Process flowsheet diagram (PFD) of the TVSA process in Aspen Adsorption.

Table 4. Process cycle durations for the base case.

Cycles of Process	Unit	Duration
Adsorption	s	7200
Evacuation	s	6
Heating+ Evacuation	s	10000
Cooling	s	Temperature matched the feed temperature
Pressurising	s	Pressure matched the atmospheric pressure

Table 5. Formulas for performance indicators.

Performance Indicators	Unit	Formula
CO_2 Purity	%	$\frac{\int_0^{t_{cycle}} F_{product}\, y_{CO_2} dt}{\sum_{i=1}^{m} \int_0^{t_{cycle}} F_{product}\, y_i dt}$
Recovery	%	$\frac{\int_0^{tcycle} (y_{product,CO_2}\, F_{product}\big\vert_{z=L}) dt}{\int_0^{tcycle} (y_{feed,CO_2}\, F_{feed}\big\vert_{z=0}) dt}$
Productivity	Kmol/Kg.year	$\frac{3600 \times \int_0^{tcycle} (F_{product}\, y_{CO_2}) dt}{w_{adsorbent} t_{cycle}}$
SEC (vacuum)	MJ/Kg CO_2	$\frac{\int_0^{t_{cycle}} \frac{F_{vac} P_{vac} \gamma}{\eta(\gamma-1)} \left[(\frac{P_{feed}}{P_{vac}})^{1-\frac{1}{\gamma}} - 1 \right] dt}{\int_0^{t_{cycle}} F_{product}\, y_{product,CO_2} dt}$

2.3. Performance Metrics

To evaluate the steady-state performance of the TVSA process, four key performance indicators – recovery, CO_2 purity, productivity, and specific energy consumption– are evaluated, with their respective definitions provided in Table 5. The total energy demand comprises the electrical energy required for the vacuum pump and the thermal energy for the heat exchanger. The electrical energy consumption of the vacuum pump was estimated using the corresponding thermodynamic expression shown in Table 5, with a vacuum pump efficiency (η) assumed to be 0.8. The heat capacity ratio(C_p/C_v), γ, was taken as 1.4, which is the typical value for air and CO_2. Thermal energy input associated with the heat exchanger was calculated directly using Aspen Adsorption. Given the negligible pressure drop across the bed under experimental conditions, fan energy consumption was considered insignificant and excluded from the overall energy analysis.

3. Results and Discussion

3.1. Mass Transfer Coefficient (MTC) Validation: Breakthrough Curve Comparison

To achieve accurate modelling of breakthrough dynamics, the reliability of the isotherm model was first established. Figure 2a , b, and c demonstrates the close alignment between simulated and experimental CO_2 adsorption isotherms at 25, 49, and 69 ^{0}C which are shown in different range of CO_2 partial pressure. The model also reproduces the adsorption behaviour trend at lower temperatures, supporting its suitability for DAC simulations under reduced temperature conditions. The validated isotherm model utilised to simulate breakthrough performance, which was subsequently compared with experimental data. Figure 3a presents the breakthrough curves at 23 ^{0}C and a flow rate of 17.2 N ml/min. Quantitatively, the predicted breakthrough time deviates by about 3% (Figure 3b), underscoring the model's predictive accuracy. Further validation at different inlet flow rates (Figure 4) demonstrates the model's robustness across varying operational conditions. For flow rates of 26.8, 48.6, and 100 NmL/min, the average absolute relative deviation (AARD) values were 8.18%, 7.24%, and 4.97%, the root mean squared error (RMSE) values were 2.99×10^{-5}, 3.10×10^{-5}, and 2.88×10^{-5}, and the R^2 values were 0.81, 0.72, and 0.80, respectively.

Validation against experimental breakthrough curves at different flow rates led to the adjustment of the initial estimation of the mass transfer coefficient to 0.05 S^{-1} for pressure before the step. The values of Avrami equation parameters reported in [56] effectively describe the breakthrough behaviour beyond the step pressure. The simulation results demonstrated that applying a dual-kinetic approach provides a more accurate representation of the adsorption process compared to using the LDF model alone (Figure 3a).

The LDF model captures the initial sharp breakthrough resulting from mmen-Mg_2(dobpdc)'s cooperative adsorption behaviour. This sorbent exhibits a step-shaped isotherm, where CO_2 uptake begins abruptly once a threshold partial pressure is reached. At low loading, strong exothermic chemisorption drives the rapid formation of ammonium carbamate chains, producing a steep concentration front and a sharp breakthrough transition [51]. However, the LDF model alone is not sufficient to reproduce the gradual uptake observed at the intermediate and high CO_2 loading. This later-stage behaviour is attributed to moderate chemisorption and weak physisorption, driven by enthalpy dependent-adsorption mechanisms [47].

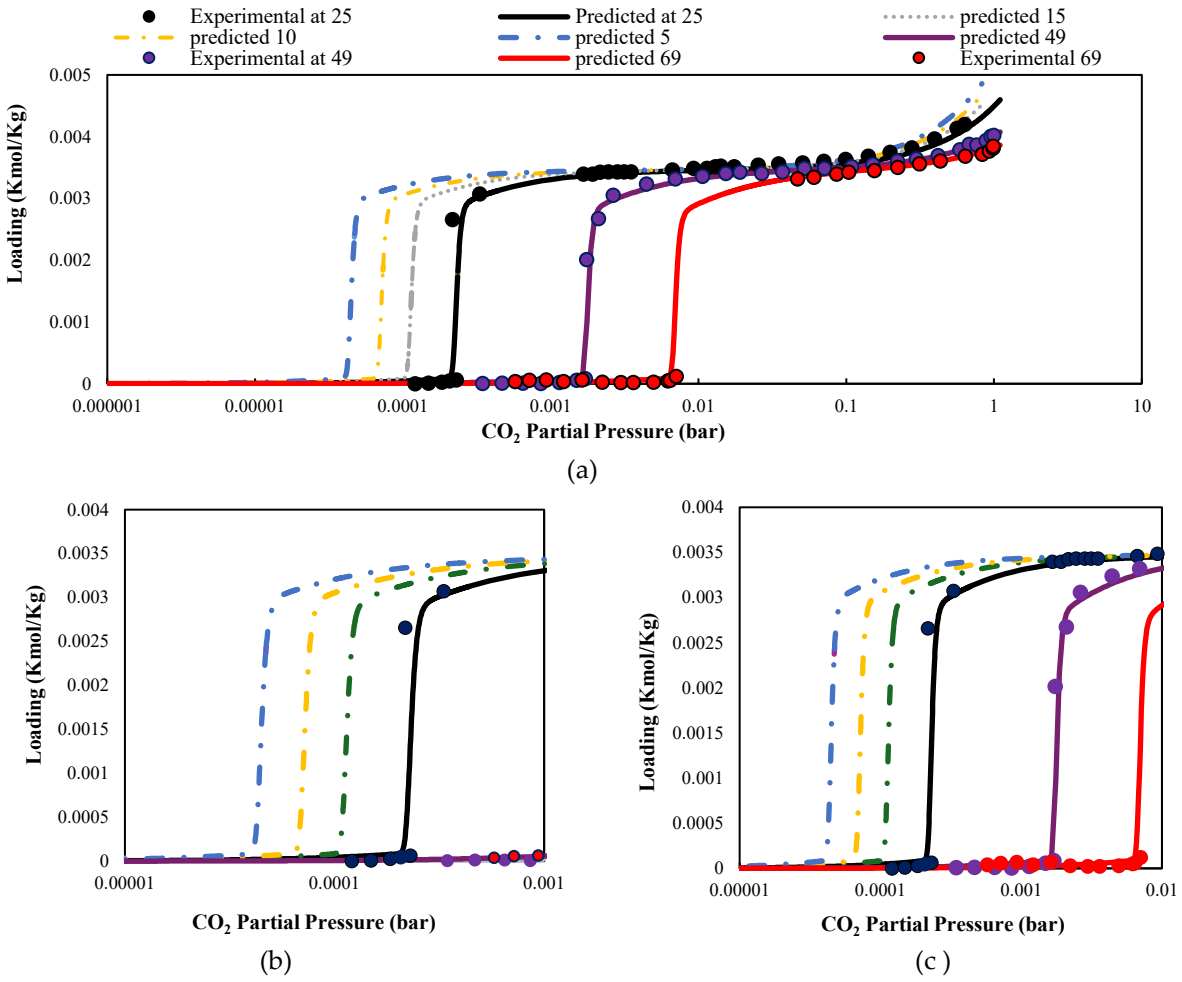

Figure 2. CO_2 pure-component adsorption isotherms plotted over different partial pressure ranges: (a) 1×10^{-6} to 10 bar, (b) 1×10^{-5} to 1×10^{-3}bar, and (c) $1\times10^{-5}$to 1×10^{-2} bar. Curves correspond to temperatures of 69 ^{0}C (red), 49 ^{0}C (purple), 25 ^{0}C (black), and model predictions at 15 ^{0}C (grey), 10 ^{0}C yellow), and 5 ^{0}C (blue). Circle markers represent experimental data.

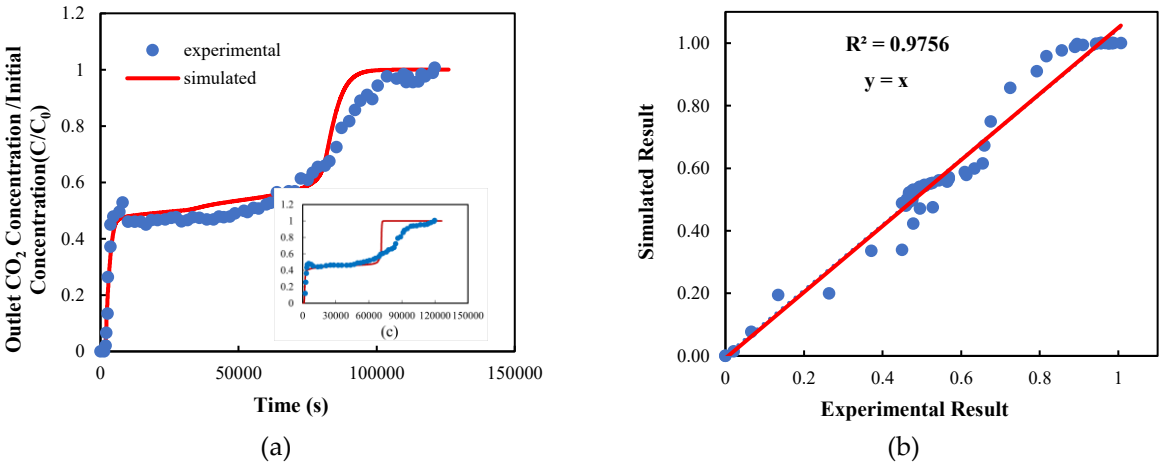

Figure 3. (a) Breakthrough curve fitting at 23 ^{0}C and flow rate of 17.2 N ml/min using the dual kinetic approach (main plot), (b) Error estimation between experimental and simulated breakthrough points for the dual kinetic approach, (c) breakthrough curve fitting using the LDF model (inset), with axis titles consistent with the main plot.

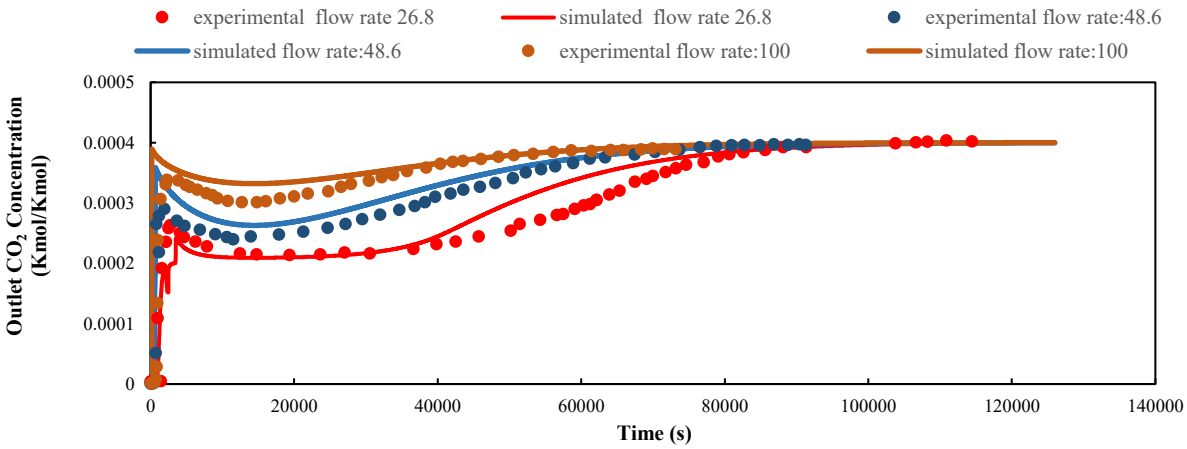

Figure 4. Breakthrough fitting at 23 ^{0}C for different flow rates. Circle points show experimental data and solid lines represent simulated results. Red, blue, and orange correspond to flow rates of 26.8, 48.6, and 100 Nml/min, respectively.

3.2. Parametric Evaluation

The performance of mmen-Mg_2(dobpdc) in DAC is governed by its relatively slow adsorption kinetics and step-shaped isotherm. While the sorbent exhibits high theoretical CO_2 capacity, enhancing recovery depends not only on its intrinsic uptake potential but also on its kinetics behaviour. At ambient CO_2 concentration, adsorption proceeds in two distinct stages: an initial chemisorption phase with slower kinetics, followed by a faster cooperative insertion step at higher loading. These kinetic characteristics result in a sharp breakthrough followed by a gradual saturation phase, leading to prolonged adsorption times. Therefore, carful tunning of process parameters is essential to enable the sorbent to approach equilibrium loading. A systematic investigation of key process parameters such as feed flow rate, temperature, and step durations are critical to overcoming mass transfer limitations and improving overall process performance.

This section evaluates the effects of ambient temperature, inlet flow rate, vacuum pressure, heat exchanger temperature, and step durations on the performance of the DAC process. Parametric analysis provides a systematic framework for assessing the sensitivity of system outputs to these variables and defining optimal conditions for improving process efficiency. A related techno-economic analysis of solid-sorbent DAC systems demonstrated how variations in process conditions and bed geometry affect both energy requirements and cost, highlighting the importance of identifying the most influential parameters to balance CO_2 capture efficiency with operational feasibility [72]. The results of this study identify effective operating windows and illustrate the trade-offs among CO_2 recovery, specific energy consumption, and system scalability under varying conditions.

3.2.1. Adsorption Time

During the adsorption step, the primary objective is to maximise CO_2 uptake and achieve full bed saturation [73]. This study examines the effect of extending the adsorption time from 5000 to 10000 Seconds on overall process efficiency. While saturation is consistently achieved at nodes 1 and 10 - representing the inlet and midpoint of the bed- the saturation level at node 20- located near the bed outlet- increases with longer adsorption durations. As shown in Figure 5, full saturation at node 20 is attained only when the adsorption time exceeds 9000 seconds, indicating improved bed utilisation with extended adsorption period. The prolonged bed saturation is primarily attributed to the limited CO_2 mass transfer rate of the sorbent, as reflected in the breakthrough curve profile. As shown in Figure 3a, the curve exhibits a distinct plateau phase following the initial breakthrough

front, during which CO_2 continues to adsorb gradually, particularly in the downstream segments of the bed. This observation aligns with the work of Stampi-Bombelli et al. [73], who argued that, due to the inherently slow CO_2 mass transfer in DAC processes, the adsorption step should be sufficiently long to ensure saturation of the entire column. They proposed defining adsorption time based on the saturation of the final bed segment rather than relying solely on breakthrough time, particularly because, in DAC systems, the CO_2 recovery constraint is less stringent than in post-combustion capture, allowing for longer adsorption durations to prioritise bed saturation.

However, this extended adsorption period introduces a trade-off: While longer adsorption times improve bed utilisation and allow the bed to approach full saturation, they also coincide with the plateau region of the breakthrough curve, where the adsorbent is no longer able to capture all incoming CO_2. Consequently, CO_2 recovery slightly decreases by approximately 2%. As shown in Figure 6, increasing the adsorption time enhances specific energy consumption and CO_2 purity, with both metrics plateauing around 9000 seconds, signifying that the system approaches equilibrium and the adsorption bed is saturated with CO_2 (Figure 5). Meanwhile, beyond 9000 seconds, process productivity declines as fewer operational cycles can be completed annually. This reflects a performance limitation; while prolonging the adsorption phase initially improves overall performance; it eventually leads to diminishing returns in both productivity and CO_2 recovery.

3.2.2. Desorption Temperature

In a TVSA process, regeneration of the adsorbent is achieved by applying both elevated temperature and reduced pressure, which together enhance the thermodynamic driving force for CO_2 desorption [57,73,74]. Therefore, the selection and optimisation of desorption temperature and vacuum pressure are closely interdependent.

Figure 7a and b present the effect of desorption temperature under a fixed vacuum pressure (P_{eva}= 0.09 bar) on performance indexes. As shown, CO_2 recovery and productivity remain negligible at temperatures around 100 ^{0}C but increase sharply once a specific threshold temperature is reached, approximately 120 ^{0}C. However, increasing the desorption temperature beyond 120 ^{0}C has minimal impact on further improving process performance, reflecting the cooperative desorption mechanism of mmen-Mg_2(dobpdc) associated with its characteristic step-shaped isotherm and temperature-dependent kinetics. These frameworks exhibit long induction periods near the step temperature, with desorption only becoming significant once a critical temperature is reached [75]. Importantly, the desorption threshold temperature is influenced by the applied vacuum level. Under deeper vacuum pressure, the equilibrium partial pressure of CO_2 decreases, enabling desorption at lower temperatures [76]. These findings establish a practical threshold that can guide the optimisation of regeneration strategies in DAC systems employing this sorbent.

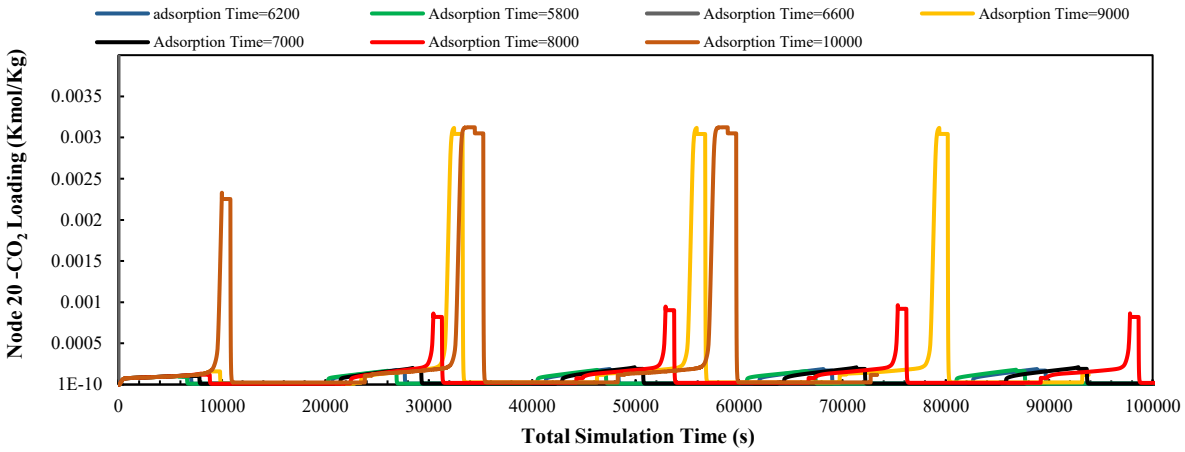

Figure 5. CO_2 loading at the bed outlet (node 20) as a function of total simulation time (adsorption + desorption), extending until equilibrium is reached. Each curve corresponds to a different adsorption duration: 5800 s (green), 6200 s (dark blue), 6600 s (purple), 7000 s (black), 8000 s (red), 9000 s (yellow), and 10000 s (brown).

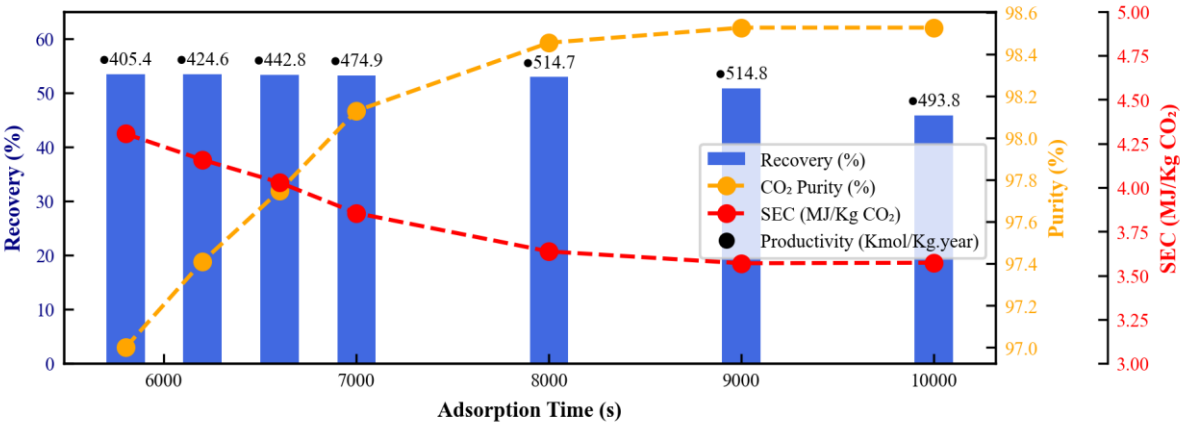

Figure 6. Effect of adsorption time on process performance indicators. The column plot represents recovery (%) with numerical values above each column indicating productivity (kmol CO_2/Kg·year). The two dashed lines correspond to CO_2 purity (%) (yellow) and specific energy consumption (MJ/Kg CO_2) (red).

3.2.3. Desorption Time

Figure 8a and b illustrate the variation in productivity, CO_2 purity, recovery and specific energy consumption across different desorption durations under a constant evacuation pressure (P_{eva}= 0.09). Extending the desorption time beyond 500 seconds has minimal impact on specific energy consumption (which remains nearly constant) and CO_2 recovery (which stabilises around 52.8% - 53.2%) since the bed reaches its target temperature early in the desorption stage, and both metrics subsequently stabilise. However, desorption time shows a more significant influence on CO_2 purity and overall process productivity. Increasing the duration up to 2000 seconds improves purity, as more CO_2 is removed from the bed. Beyond this point, further improvement in purity is negligible (< 0.2%), indicating that the sorbent's desorption capacity is nearly exhausted at 120 ^{0}C. Meanwhile, longer desorption times reduce the number of process cycles that can be completed annually, thereby decreasing overall productivity. Previous studies have demonstrated that an optimal desorption duration exists that maximises CO_2 yield with minimal energy input [73]. Similarly, findings from multi-objective optimisations of TVSA cycles using amine-functionalised solid sorbents show that prolonged desorption offers diminishing returns in

terms of purity and recovery, while significantly reducing productivity due to extended cycle times [77]. Moreover, Figure 9 shows the variation in productivity with desorption temperatures between 120 and 170 ^{0}C across desorption durations ranging from 2000 to 12000 seconds. The curve indicates that the desorption temperature exceeds the identified threshold (~120 ^{0}C), making the desorption duration increasingly influential. In this regime, rather than further increasing the temperature, reducing the desorption time becomes a more effective strategy for improving annual productivity without compromising separation performance.

3.2.4. Evacuation Pressure

One of the important objectives of DAC processes is to achieve high CO_2 purity, ensuring that the captured product meets the quality requirements for downstream applications. This necessitates the effective removal of residual air from the adsorption bed before initiating the desorption step. Moreover, this step also helps prevent oxygen-induced degradation of amine-functionalised sorbents during subsequent heating [78].

Figure 10a and b compare CO_2 purity, productivity, specific energy consumption, and recovery for different evacuation pressures, ranging from 0.07 to 0.4 bar. As shown in the figures, there is a gradual reduction in purity, recovery, and productivity with increasing vacuum pressure up to 0.15 bar, followed by a more pronounced drop beyond this point. Additionally, a slight trade-off exists between specific energy consumption and CO_2 purity, recovery, and productivity. while operating at higher vacuum pressures reduces the energy demand of the vacuum pump– thereby reducing specific energy consumption– this benefit becomes less significant beyond 0.15 bar, as the weakened desorption driving force leads to a decline in CO_2 recovery. The findings indicate that lower evacuation pressures significantly enhance CO_2 recovery, purity and productivity by enabling more complete regeneration of the sorbent. This improvement is attributed to the stronger thermodynamic driving force for desorption at lower pressures, which facilitates more efficient CO_2 release from the adsorbent [73]. By increasing the pressure differential between the adsorbed CO_2 and the surrounding gas phase, lower evacuation pressures enhance the effectiveness of sorbent regeneration. However, the energy savings achieved at higher vacuum pressures are offset by corresponding reduction in recovery and productivity.

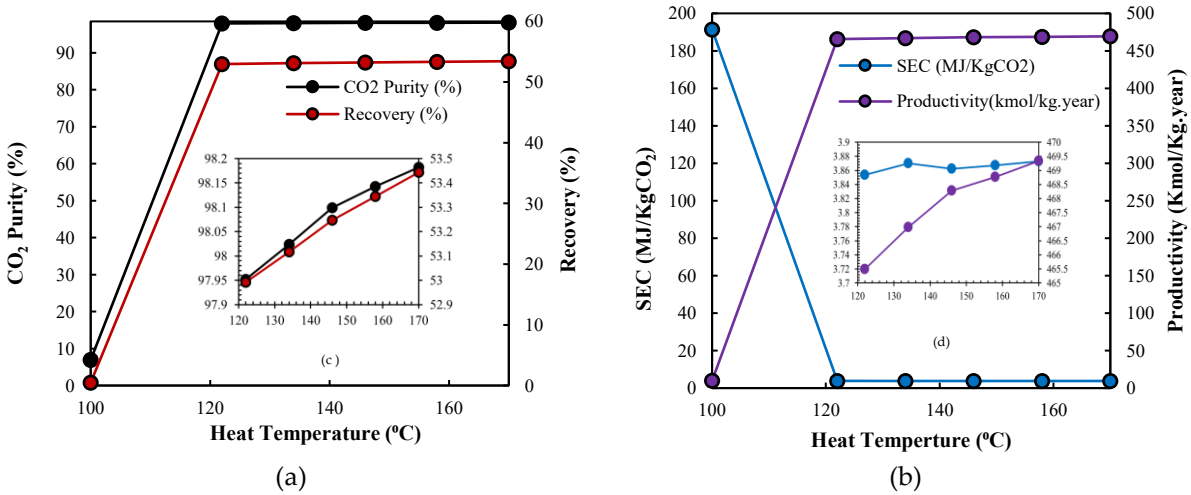

Figure 7. Effect of different heating temperatures during the desorption stage on performance indicators. Panels (a) and (b) show temperature ranges from 100–170 ^{0}C, while panels (c) and (d) zoom in on the range of 120–170 ^{0}C, with axis titles consistent with the main figures. (a) CO_2 purity (%) and recovery (%) are represented by black and red lines, respectively (b) Productivity

(Kmol CO_2/Kg·year) and specific energy consumption (MJ/Kg CO_2) are shown by purple and blue lines, respectively.

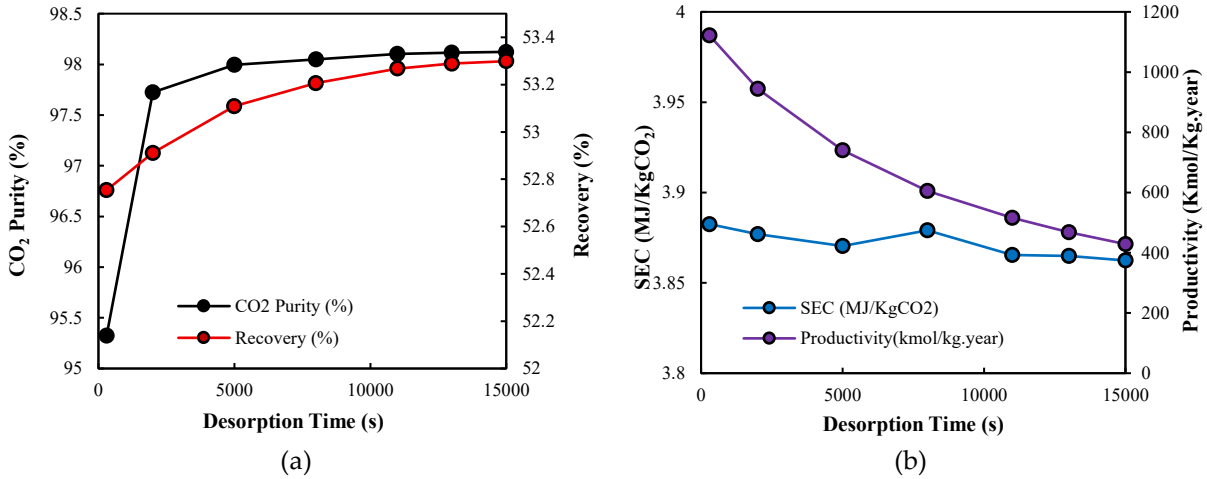

Figure 8. Effect of desorption time on performance indicators over the range of 300 to 1500 seconds. (a) CO_2 purity (%) and recovery (%) are shown by black and red lines, respectively. (b) productivity (Kmol CO_2/Kg·year) and specific energy consumption (MJ/Kg CO_2) are shown by purple and blue lines, respectively.

3.2.5. Inlet Feed Temperature

The effect of feed temperature on CO_2 purity, recovery, productivity, and specific energy consumption is investigated to consider different ranges of environmental temperatures. According to the simulation results in Figure 11a and b, CO_2 purity, recovery, and productivity remain relatively stable at feed temperatures below 20 ^{0}C. As the temperature increases beyond this point, all three performance indicators exhibit a consistent downward trend. This suggests that lower ambient (feed) temperatures are more favourable for achieving optimal DAC process performance using mmen-Mg_2(dobpdc), particularly in maintaining high product purity and maximising sorbent utilisation.

This behaviour can be attributed to the thermodynamics of the sorbent's cooperative adsorption mechanism, in which CO_2 is captured through insertion into metal-amine bonds, forming extended chains of ammonium carbamate along the one-dimensional channels [49,79]. This process is exothermic and highly temperature-sensitive [49]. As a result, at elevated temperatures, the formation of ammonium carbamate chains becomes thermodynamically less favourable, reduced CO_2 uptake and diluted product streams. This trend was also observed by Martell et al. [75], who reported more favourable adsorption kinetics and thermodynamics at lower temperatures due to cooperative chemisorption mechanisms in diamine-appended Mg_2(dobpdc) frameworks.

Higher feed temperatures also lead to increased specific energy consumption. This is primarily due to the reduced amount of CO_2 captured, which outweighs the benefit of lower heating energy input required to reach the target desorption (Figure 11b).

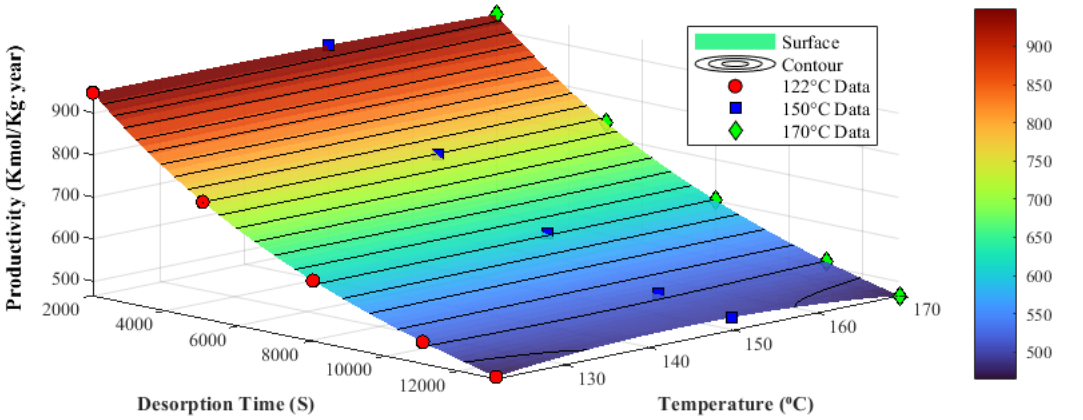

Figure 9. Effect of desorption temperature on productivity (Kmol CO_2/Kg·year) for different desorption durations (2000 -12000 seconds) over a temperature range of 120 to 170 ^{0}C.

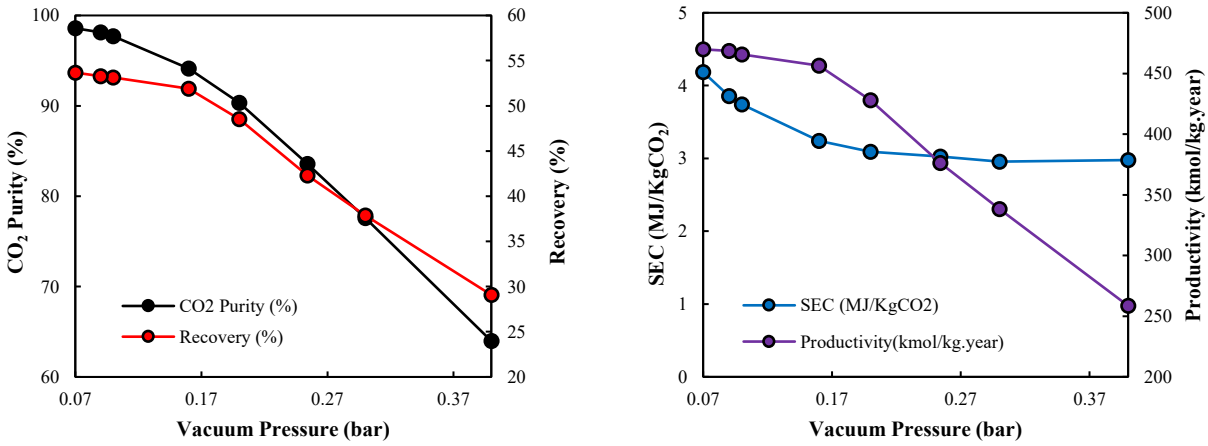

(a) (b)

Figure 10. Effect of vacuum pressure (0.07–0.3 bar) on DAC performance indicators. (a) CO_2 purity (%) and recovery (%) are shown by black and red lines, respectively. (b) productivity (Kmol CO_2/Kg·year) and specific energy consumption (MJ/Kg CO_2) are shown by purple and blue lines, respectively.

3.2.6. Inlet Feed Flow rate

The sensitivity analysis on feed flow rate, conducted under constant feed temperature (23 ^{0}C) and evacuation pressure (0.09 bar), reveals that increasing the inlet air flow rate beyond 0.0004 Kmol/h has a minimal influence on CO_2 purity, productivity, and specific energy consumption. However, a significant decline in CO_2 recovery is observed (column plot in Figure 12. This reduction is attributed to insufficient gas residence time within the adsorption bed, which restricts CO_2 diffusion and hinders effective adsorption onto the sorbent surface. Consequently, a significant fraction of CO_2 bypasses the bed without being captured. Conversely, at lower flow rates, extended gas-solid contact time enables the sorbent to approach full saturation, thereby improving CO_2 recovery. The stability of CO_2 purity, specific energy consumption, and productivity at higher flow rates can be explained by the dynamic balance between adsorption kinetics and process throughput. Although increasing the flow rate reduces contact time, the high velocity also increases the mass transfer driving force, allowing CO_2 to be quickly adsorbed.

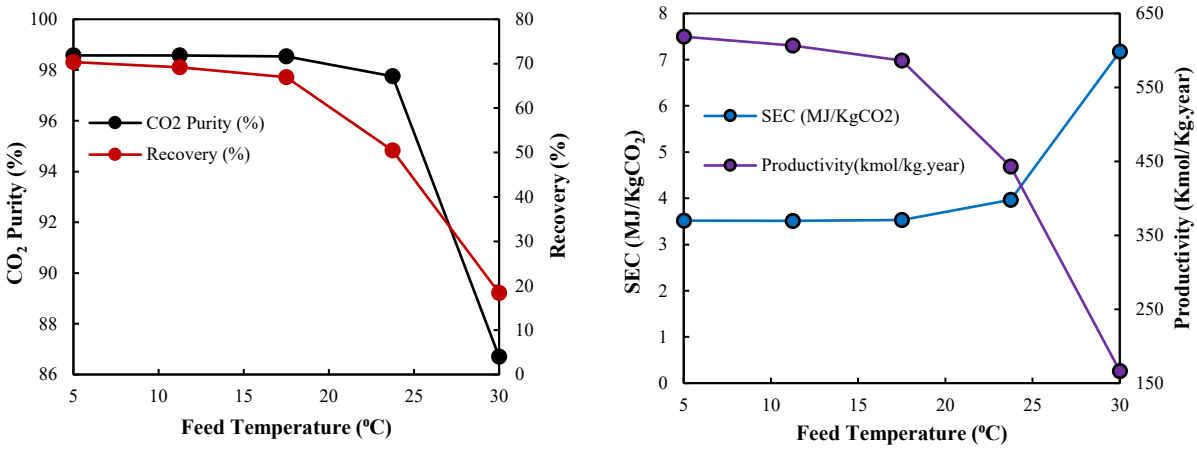

Figure 11. a) Effect of different feed temperatures (5-30 ºC) on performance indicators. (a) CO_2 purity (%) and recovery (%) are shown by black and red lines, respectively. (b) productivity (Kmol CO_2/Kg·year) and specific energy consumption (MJ/Kg CO_2) are shown by purple and blue lines, respectively.

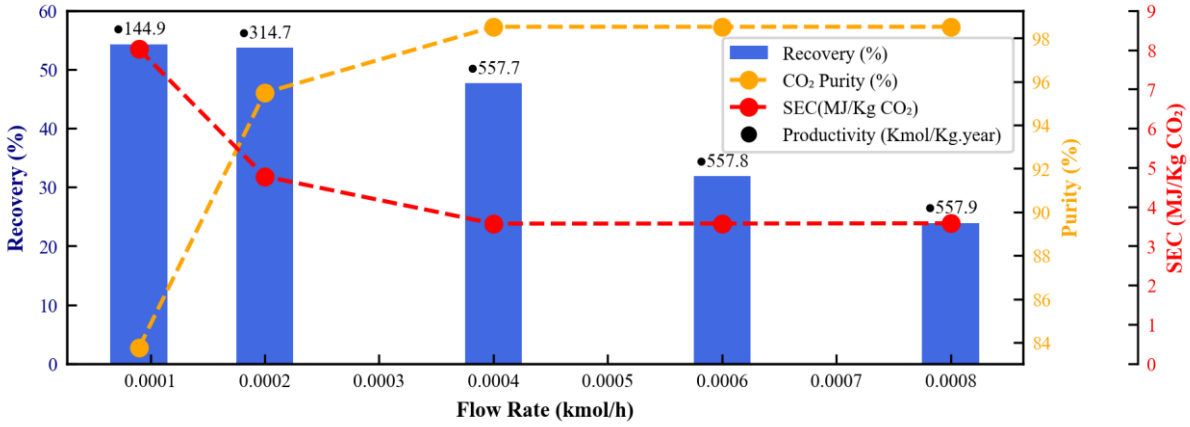

Figure 12. Effect of different feed flow rates on process performance indicators. The column plot represents recovery (%) with numerical values above each column indicating productivity (Kmol CO_2/Kg·year). The two dashed lines correspond to CO_2 purity (%) (yellow) and specific energy consumption (MJ/Kg CO_2) (red).

3.3. Optimal Design Discussion

To complement the individual parameter investigations, a normalised sensitivity analysis was conducted to compare the relative impact of each process parameter on four key performance indicators: SEC, CO_2 purity, recovery, and productivity. The study considered the following parameter ranges: adsorption time (5000-10000 seconds), desorption time (300-15000 seconds), feed temperature (5-30 ºC), feed flow rate (0.0001-0.0008 Kmol/h), and vacuum pressure (0.07-0.4 bar). According to Figure 13, feed temperature consistently demonstrates a strong influence across all metrics, significantly affecting SEC, recovery, and productivity. Its role in controlling the thermal and mass transport within the bed makes it particularly impactful. Vacuum pressure also strongly influences recovery and purity, as it governs the thermodynamic driving force for CO_2 desorption. Desorption time significantly affects productivity by limiting the number of annual operational cycles, while also influencing CO_2 purity through its impact on bed regeneration. By contrast, adsorption time shows minimal influence across all indicators in the

sensitivity analysis, indicating that once sufficient bed saturation is achieved, further increase in adsorption time have a negligible effect on system performance. Finally, heating temperature appears to have a minimal impact in this analysis, which aligns with prior findings in Section 3.2.2, where it was demonstrated that heating temperatures above 120 ^{0}C do not substantially improve performance due to the system reaching equilibrium; hence, the effect of further increases within the 120–170 ^{0}C range is limited.

Translating the insights from the sensitivity analysis into process improvements, the base case performance is compared with optimised condition performance. Table 6 succinctly summarises the resulting performance indicators for both the baseline and optimised scenario. The optimised configuration demonstrates substantial enhancement over the base case. Specifically, it achieves a significant improvement in CO_2 recovery (from 53.26 to 75%) and productivity (from 474.85 to 1373 Kmol/Kg.year). Crucially, these gains are realised while maintaining a consistently high CO_2 purity of 98% and notably reducing the specific energy consumption from 3.85 to 3.64 MJ/Kg CO_2. These improvements are primarily attributable to strategic adjustments in operating conditions, including a reduction in vacuum pressure to 0.08 bar, a decrease in desorption time to 1000 Seconds, an extension of adsorption time to 8200 seconds, and lowering the feed temperature to below 7 ^{0}C. These adjustments align directly with the sensitivities identified for each parameter and collectively support the development of more energy-efficient and sustainable DAC systems.

To further contextualise the performance of our developed system, Table 6 also incorporates a comparison with three established benchmark sorbents reported in the DAC literature. one of these is Lewatit VP OC 1065, evaluated under a packed bed TVSA process, which closely aligns with our system's bed configuration and process type. The other two sorbent, Mmen-Mg_2(dobpdc) and MIL-101(cr)-PEI-800, employing novel coated monolith adsorption beds. Additionally, the table presents performance data from the Climeworks commercial DAC process to provide broader industrial benchmark.

This analysis focuses on purity, recovery, and specific energy consumption, providing a comprehensive assessment of the system's operational efficiency and effectiveness. Our optimised system highlights competitive capabilities, particularly in achieving lower specific energy consumption alongside enhanced purity and recovery rates. These improvements indicate the potential for reduced operational costs and increased process sustainability. The calculated energy requirement in our benchmark case is approximately 59% lower than the reported value for the Climeworks system. This deviation is anticipated, as our model represents a highly idealised and optimised scenario. For example, Climeworks adsorption bed configuration [80] likely limits full bed saturation due to practical design constraints, whereas our simulation assumes optimal sorbent utilisation. Several additional factors contribute to this difference:

- Current model assumes negligible pressure drop, thereby excluding blower energy consumption.
- Real-world vacuum equipment typically operates at lower efficiencies than assumed in ideal models.
- Climeworks contactor design include additional flow resistance due to the parallel flow path through structured adsorbent sheets, whereas current model assumes axial flow through a thin sorbent layer, reducing resistance and energy loss.
- Current study does not consider the presence of water in the feed and associated energy required for water-CO_2 separation. These factors would likely increase the energy demand in real word systems.

Among the benchmark sorbents considered, the Lewatit VP OC 1065, evaluated by Deschamps etal. [81], stands out for its relatively high energy consumption despite

operating under idealised process conditions. This can be attributed, in part, to the inclusion of moisture and its interactions with CO_2, a level of complexity not considered in current study. Additionally, the sorbent demonstrates the ability to achieve high CO_2 purity without the need for deep vacuum conditions.

Furthermore, the study by Sinha et al. [53] investigated mmen-Mg_2(dobpdc) and MIL-101(cr)-PEI-800 under experimental conditions using a monolithic adsorption configuration. The predicted energy consumption for mmen-Mg_2(dobpdc) in their study is slightly lower than that reported in the present study. This variation can be attributed to differences in bed configuration and the higher CO_2 purity achieved in our system, which is facilitated by operating at deeper vacuum levels. Although such conditions increase energy demand, they also enhance separation performance. In contrast, the use of MIL-101(cr)-PEI-800 in monolithic configurations results in substantially higher energy consumption and lower CO_2 recovery, indicating that this sorbent may be less promising candidates for DAC applications compared to mmen-Mg_2(dobpdc) under the applied condition.

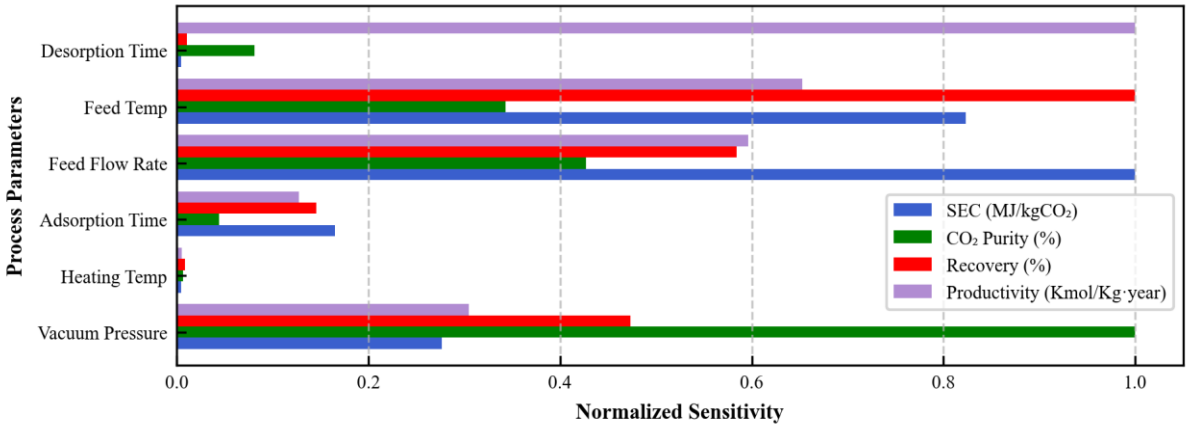

Figure 13. Sensitivity analysis of six process parameters on key performance indicators: CO_2 purity, recovery, specific energy consumption and productivity.

Table 6. Performance comparison of the optimised mmen-Mg_2(dobpdc) packed bed TVSA system with established benchmark sorbents for DAC.

Performance Indicators	Process	Purity	Recovery	Specific Energy Consumption	Productivity	Reference
Unit		%	%	MJ/Kg	Kmol/Kg.year	
Base case	Packed bed, TVSA	98.13	53.26	3.85	474.85	This work
Designed case	Packed bed, TVSA	98.05	75	3.64	1373	This work
Climeworks-Amine-based sorbent	TVSA	99.9	85.4	6.12-8.18	1344	[82,83]
Lewatit VP OC 1065	Packed bed, TVSA	99	77	5.42	1090	[81]
Mmen-Mg_2(dobpdc)	Coated monolith Steam assistance-TVSA	95	60	3.52	-	[53]
MIL-101(cr)-PEI-800	Coated monolith Steam assistance-TVSA	95	50	5.34	-	[53]

4. Conclusion and Prospect

This study evaluates the performance of mmen-Mg_2(dobpdc) under realistic DAC process conditions using a dynamic simulation framework. This metal-organic framework, known for its distinctive step-shaped isotherm, was evaluated within a TVSA process in Aspen Adsorption. After validating the simulation model against experimental breakthrough data and confirming its reliability, a sensitivity analysis was conducted to identify the most influential process parameter (vacuum pressure, adsorption and desorption times, feed temperature, feed flow rate, and heat exchanger temperature) on CO_2 purity, recovery, productivity, and specific energy consumption. Beyond demonstrating high CO_2 purity and recovery, the analysis highlights the complex and interdependent relationships between process variables and their implication for system performance and design.

A key insight from this work is the trade-off between CO_2 recovery and productivity. While lower feed temperatures and extended adsorption time enhance recovery by increasing sorbent loading and saturation levels, they concurrently reduce the frequency of adsorption- desorption cycles, thus lowering productivity. Another significant finding is the dual role of vacuum pressure: deeper vacuums improve desorption efficiency and boost both CO_2 purity and recovery. However, this comes at the expense of increased SEC, particularly from mechanical work. The interplay between feed temperature and vacuum pressure is particularly noteworthy- lower feed temperature shifts the isotherm's step-pressure downward, enabling effective desorption at milder vacuum conditions, and thus offering potential energy saving if properly tuned. This study also reveals a threshold effect for desorption temperature, beyond which further heating yields marginal benefit. At deeper vacuum level, effective regeneration can occur at lower temperatures, provided sufficient desorption time is allowed. This introduces a critical design trade-off longer desorption times reduce thermal energy demand (lowering SEC), but again, may compromise overall productivity.

Although the current study was conducted at an experimental scale and did not explicitly account for humidity fluctuations or long-term material stability, the demonstrated performance underscores the potential of this sorbent for DAC applications. These results provide a robust foundation for sustainable DAC process development, offering guidance for future research aimed at optimising the process and improving system scalability. Future investigation is needed into sorbent degradation mechanism under cyclic operation, as well as the scalability of the adsorption bed design for industrial-scale development. Further work will also prioritise a comprehensive evaluation of competitive adsorption between H_2O and CO_2 under realistic atmospheric conditions. Furthermore, the insights gained from this study reveal the interconnected dynamics among process variables, highlighting the limitations of isolated parameter tunning and emphasising the need for system-level optimisation. The complexity of balancing CO_2 purity, recovery, SEC, and productivity justifies the application of advanced multi-objective optimisation techniques to define operating strategies that achieve optimal performance across these key indicators and support the development of sustainable carbon removal technologies.

References

[1] H. R. Nasriani and M. Jamiolahmady, "Maximizing fracture productivity in unconventional fields; analysis of post hydraulic fracturing flowback cleanup," *J Nat Gas Sci Eng*, vol. 52, no. September 2017, p., 2018, doi: https://doi.org/10.1016/j.jngse.2018.01.045.

[2] H. R. Nasriani and A. Kalantari Asl, "Choke Performance in High-rate Gas Condensate Wells Under Subcritical Flow Condition," *Energy Sources, Part A: Recovery, Utilization, and Environmental Effects*, vol. 37, no. 2, pp. 192–199, 2014, doi: 10.1080/15567036.2011.582607.

[3] H. R. Nasriani, M. Jamiolahmady, T. Saif, and J. Sánchez, "A systematic investigation into the flowback cleanup of hydraulic-fractured wells in unconventional gas plays," *Int J Coal Geol*, vol. 193, 2018, doi: 10.1016/j.coal.2018.04.012.

[4] H. R. Nasriani and M. Jamiolahmady, "A Comparison of Clean-Up Efficiency of Multiple Fractured Horizontal Wells and Hydraulically Fractured Vertical Wells in Tight Gas Reservoirs," in *SPE Europec featured at 80th EAGE Conference and Exhibition*, Society of Petroleum Engineers, Jun. 2018. doi: 10.2118/190862-MS.

[5] H. R. Nasriani and M. Jamiolahmady, "Optimising Flowback Strategies in Unconventional Reservoirs: The Critical Role of Capillary Forces and Fluid Dynamics," *Energies (Basel)*, vol. 17, no. 23, p. 5822, Nov. 2024, doi: 10.3390/en17235822.

[6] F. Joan Medaiyese, H. Reza Nasriani, K. Khan, and L. Khajenoori, "Sustainable Hydrogen Production from Plastic Waste: Optimizing Pyrolysis for a Circular Economy," *Hydrogen*, 2025, doi: 10.3390/hydrogen6010015.

[7] F. J. Medaiyese, H. R. Nasriani, L. Khajenoori, K. Khan, and A. Badiei, "From Waste to Energy: Enhancing Fuel and Hydrogen Production through Pyrolysis and In-Line Reforming of Plastic Wastes," Jun. 02, 2024, *Multidisciplinary Digital Publishing Institute (MDPI)*. doi: 10.3390/su16124973.

[8] E. Joonaki, E. Rostaminikoo, S. Ghanaatian, and H. R. Nasriani, "Thermodynamic properties of hydrogen containing systems and calculation of gas critical flow factor," in *Measurement: Sensors*, Elsevier Ltd, 2025. doi: 10.1016/j.measen.2024.101587.

[9] S. Gholami, E. Rostaminikoo, L. Khajenoori, and H. R. Nasriani, "Density determination of CO2-Rich fluids within CCUS processes," in *Measurement: Sensors*, Elsevier Ltd, 2025. doi: 10.1016/j.measen.2024.101739.

[10] E. Rostaminikoo, S. Ghanaatian, E. Joonaki, H. R. Nasriani, and J. Whitton, "Advanced thermodynamics of hydrogen and natural gas blends for gas transmission and distribution networks," in *Measurement: Sensors*, Elsevier Ltd, 2025. doi: 10.1016/j.measen.2024.101765.

[11] E. Joonaki, E. Rostaminikoo, S. Ghanaatian, and H. Nasriani, "Thermodynamics of Hydrogen; Analysing and Refining of Critical Flow Factor Through Comprehensive Uncertainty Assessment and Experimental Data Integration," in *ADIPEC*, SPE, Nov. 2024. doi: 10.2118/222973-MS.

[12] IEA (2024), "Clean Energy Market Monitor," Paris, Mar. 2024. [Online]. Available: https://www.iea.org/reports/clean-energy-market-monitor-march-2024

[13] Theo Stein, "No sign of greenhouse gases increases slowing in 2023," Apr. 2024. Accessed: Apr. 05, 2024. [Online]. Available: https://research.noaa.gov/no-sign-of-greenhouse-gases-increases-slowing-in-2023/

[14] M. Ozkan and R. Custelcean, "The status and prospects of materials for carbon capture technologies," *MRS Bull*, vol. 47, no. 4, pp. 390–394, Apr. 2022, doi: 10.1557/s43577-022-00364-9.

[15] UNFCCC, "Key aspects of the Paris Agreement," in *COP21/CMP11*, Paris: UNFCCC, Dec. 2015. [Online]. Available: https://unfccc.int/

[16] K. Lackner, A. Hans-Joachim Ziock, P. Grimes, and G. Associates, "Carbon Dioxide Extraction From &r: Is It An Option?," Los A: 24th Annual Technical Conference on Coal Utilization and Fuel Systems, Clearwater, Feb. 1999. Accessed: Feb. 01, 1999. [Online]. Available: https://www.osti.gov/biblio/770509

[17] R. Custelcean, "Direct Air Capture of CO 2 Using Solvents," vol. 41, p. 25, 2025, doi: 10.1146/annurev-chembioeng.

[18] F. Zeman, "Energy and material balance of CO2 capture from ambient air," *Environ Sci Technol*, vol. 41, no. 21, pp. 7558–7563, Nov. 2007, doi: 10.1021/es070874m.

[19] K. An, A. Farooqui, and S. T. McCoy, "The impact of climate on solvent-based direct air capture systems," *Appl Energy*, vol. 325, p. 119895, Nov. 2022, doi: 10.1016/J.APENERGY.2022.119895.

[20] "Evgeny A. Pidko", "Sarah Couck", "Tom Remy", "Emiel J. M. Hensen", "Bert M. Weckhuysen", "Joeri Denayer", "Jorge Gascon", "Freek Kapteijn" "Eli Stavitski," "Complexity behind CO2 Capture on NH2-MIL-53(Al)," *Langmuir*, vol. 27, no. 7, pp. 3970–3976, 2011.

[21] A. Gandomkar, F. Torabi, H. R. Nasriani, and R. M. Enick, "Decreasing Asphaltene Precipitation and Deposition during Immiscible Gas Injection Via the Introduction of a CO2-Soluble Asphaltene Inhibitor," *SPE Journal*, pp. 1–13, May 2023, doi: 10.2118/214698-PA.

[22] A. Gandomkar, H. Reza Nasriani, R. M. Enick, and F. Torabi, "The effect of CO2-philic thickeners on gravity drainage mechanism in gas invaded zone," *Fuel*, vol. 331, Jan. 2023, doi: 10.1016/j.fuel.2022.125760.

[23] H. R. Nasriani, A. A. Borazjani, B. Iraji, and M. MoradiDowlatAbad, "Investigation into the effect of capillary number on productivity of a lean gas condensate reservoir," *J Pet Sci Eng*, vol. 135, pp. 384–390, 2015, doi: 10.1016/j.petrol.2015.09.030.

[24] P. Mehra and A. Paul, "Decoding Carbon-Based Materials' Properties for High CO2 Capture and Selectivity," *ACS Omega*, vol. 7, no. 38, pp. 34538–34546, Sep. 2022, doi: 10.1021/acsomega.2c04269.

[25] S. Acevedo, L. Giraldo, and J. C. Moreno-Piraján, "Adsorption of CO2 on Activated Carbons Prepared by Chemical Activation with Cupric Nitrate," *ACS Omega*, vol. 5, no. 18, pp. 10423–10432, May 2020, doi: 10.1021/acsomega.0c00342.

[26] N. Casas, J. Schell, R. Pini, and M. Mazzotti, "Fixed bed adsorption of CO 2/H 2 mixtures on activated carbon: Experiments and modeling," *Adsorption*, vol. 18, no. 2, pp. 143–161, Oct. 2012, doi: 10.1007/s10450-012-9389-z.

[27] J. Serafin *et al.*, "Direct conversion of biomass to nanoporous activated biocarbons for high CO2 adsorption and supercapacitor applications," *Appl Surf Sci*, vol. 497, p. 143722, Dec. 2019, doi: 10.1016/J.APSUSC.2019.143722.

[28] L. Wang, Z. Liu, P. Li, J. Wang, and J. Yu, "CO2 capture from flue gas by two successive VPSA units using 13XAPG," in *Adsorption*, Dec. 2012, pp. 445–459. doi: 10.1007/s10450-012-9431-1.

[29] C. K. Z. H. L. W. K. M. S. D. T. H. N. I. C. H. D. M. P. O. O. T. and K. B. Y. Shuvo Jit Datta, "CO2 capture from humid flue gases and humid atmosphere using a microporous copper silicate," *Science (1979)*, vol. 350, no. 6258, pp. 302–306, 2015.

[30] A. 'Chamila, G. 'Chamila, G. 'Oneesha, G. 'Oneesha, G. 'Sumedha, "Carbon Capture Using Porous Silica Materials. Nanomaterials (Basel)," *nanomaterials*, no. 13, Jun. 2023, doi: 10.3390/nano13142050.

[31] J. Kundu, J. F. Stilck, J. H. Lee, J. B. Neaton, D. Prendergast, and S. Whitelam, "Cooperative Gas Adsorption without a Phase Transition in Metal-Organic Frameworks," *Phys Rev Lett*, vol. 121, no. 1, Jul. 2018, doi: 10.1103/PhysRevLett.121.015701.

[32] C. Zhang, S. Sun, S. He, and C. Wu, "Direct air capture of CO2 by KOH-activated bamboo biochar," *Journal of the Energy Institute*, vol. 105, pp. 399–405, Dec. 2022, doi: 10.1016/j.joei.2022.10.017.

[33] B. Ledesma, S. Román, A. Álvarez-Murillo, E. Sabio, and J. F. González, "Cyclic adsorption/thermal regeneration of activated carbons," *J Anal Appl Pyrolysis*, vol. 106, pp. 112–117, Mar. 2014, doi: 10.1016/J.JAAP.2014.01.007.

[34] Y. Belmabkhout, R. Serna-Guerrero, and A. Sayari, "Adsorption of CO2-containing gas mixtures over amine-bearing pore-expanded MCM-41 silica: Application for gas purification," *Ind Eng Chem Res*, vol. 49, no. 1, pp. 359–365, Jan. 2010, doi: 10.1021/ie900837t.

[35] J. Guo, S. He, X. Liu, M. Xu, J. Liang, and Y. Chu, "Hydrophobic modification of walnut shell biomass-derived porous carbon for the adsorption of VOCs at high humidity," *Chemical Engineering Journal*, vol. 488, p. 150792, May 2024, doi: 10.1016/J.CEJ.2024.150792.

[36] R. Rodríguez-Mosqueda, E. A. Bramer, T. Roestenberg, and G. Brem, "Parametrical Study on CO2 Capture from Ambient Air Using Hydrated K2CO3 Supported on an Activated Carbon Honeycomb," *Ind Eng Chem Res*, vol. 57, no. 10, pp. 3628–3638, Mar. 2018, doi: 10.1021/acs.iecr.8b00566.

[37] D. G. Boer, J. Langerak, and P. P. Pescarmona, "Zeolites as Selective Adsorbents for CO2 Separation," Mar. 13, 2023, *American Chemical Society*. doi: 10.1021/acsaem.2c03605.

[38] S. M. W. Wilson and F. H. Tezel, "Direct Dry Air Capture of CO2 Using VTSA with Faujasite Zeolites," *Ind Eng Chem Res*, vol. 59, no. 18, pp. 8783–8794, May 2020, doi: 10.1021/acs.iecr.9b04803.

[39] D. Saha, Z. Bao, F. Jia, and S. Deng, "Adsorption of CO2, CH4, N2O, and N 2 on MOF-5, MOF-177, and zeolite 5A," *Environ Sci Technol*, vol. 44, no. 5, pp. 1820–1826, Mar. 2010, doi: 10.1021/es9032309.

[40] O. K. Farha *et al.*, "Metal-organic framework materials with ultrahigh surface areas: Is the sky the limit?," *J Am Chem Soc*, vol. 134, no. 36, pp. 15016–15021, Sep. 2012, doi: 10.1021/ja3055639.

[41] P. Z. Moghadam *et al.*, "Development of a Cambridge Structural Database Subset: A Collection of Metal-Organic Frameworks for Past, Present, and Future," Apr. 11, 2017, *American Chemical Society*. doi: 10.1021/acs.chemmater.7b00441.

[42] L. 'Tai ,T. T. N. 'Ramanathan, V. ' R. K. M. 'Omid, G.-N. 'George, K. H. S. 'Jian-Bin, "A scalable metal-organic framework as a durable physisorbent for carbon dioxide capture," *Science (1979)*, vol. 374, no. 6574, pp. 1464–1469, Dec. 2021, doi: 10.1126/science.abi728.

[43] S. Xiang *et al.*, "Microporous metal-organic framework with potential for carbon dioxide capture at ambient conditions," *Nat Commun*, vol. 3, 2012, doi: 10.1038/ncomms1956.

[44] C. 'Wen,Hao L. 'Wenjun, J. 'Jiarui, Y. 'Jiexin, Z. 'Liqiang, W. 'Honghui, O. 'Zechao, Z. 'Mingzhao, C. 'Xiaohui, S. 'Dingsheng, W. 'Yadong, L. 'Shenghua, "MOF Encapsulating N-Heterocyclic Carbene-Ligated Copper Single-Atom Site Catalyst towards Efficient Methane Electrosynthesis," *Angewandte Chemie*, vol. 61, no. 4, Nov. 2021, doi: https://doi.org/10.1002/anie.202114450.

[45] shenghua Chen *et al.*, "Copper Atom Pairs Stabilize *OCCO Dipole Toward Highly Selective CO2 Electroreduction to C2H4," *Angewandte Chemie International Edition*, Dec. 2024, doi: 10.1002/anie.202411591.

[46] H. Lyu *et al.*, "Carbon Dioxide Capture Chemistry of Amino Acid Functionalized Metal-Organic Frameworks in Humid Flue Gas," *J Am Chem Soc*, vol. 144, no. 5, pp. 2387–2396, Feb. 2022, doi: 10.1021/jacs.1c13368.

[47] J. Hack, N. Maeda, and D. M. Meier, "Review on CO2Capture Using Amine-Functionalized Materials," Nov. 08, 2022, *American Chemical Society*. doi: 10.1021/acsomega.2c03385.

[48] F. Liu, S. Wang, G. Lin, and S. Chen, "Development and characterization of amine-functionalized hyper-cross-linked resin for CO2 capture," *New Journal of Chemistry*, vol. 42, no. 1, pp. 420–428, 2018, doi: 10.1039/c7nj03421k.

[49] T. M. McDonald, W. R. Lee, J. A. Mason, B. M. Wiers, C. S. Hong, and J. R. Long, "Capture of carbon dioxide from air and flue gas in the alkylamine-appended metal-organic framework mmen-Mg 2(dobpdc)," *J Am Chem Soc*, vol. 134, no. 16, pp. 7056–7065, Apr. 2012, doi: 10.1021/ja300034j.

[50] L. A. Darunte, Y. Terada, C. R. Murdock, K. S. Walton, D. S. Sholl, and C. W. Jones, "Monolith-Supported Amine-Functionalized Mg2(dobpdc) Adsorbents for CO2 Capture," *ACS Appl Mater Interfaces*, vol. 9, no. 20, pp. 17042–17050, May 2017, doi: 10.1021/acsami.7b02035.

[51] T. M. McDonald *et al.*, "Cooperative insertion of CO2 in diamine-appended metal-organic frameworks," *Nature*, vol. 519, no. 7543, pp. 303–308, Mar. 2015, doi: 10.1038/nature14327.

[52] S. Bose *et al.*, "Suitability of a diamine functionalized metal-organic framework for direct air capture," *Chem Sci*, vol. 14, no. 35, pp. 9380–9388, Aug. 2023, doi: 10.1039/d3sc02554c.

[53] A. Sinha, L. A. Darunte, C. W. Jones, M. J. Realff, and Y. Kawajiri, "Systems Design and Economic Analysis of Direct Air Capture of CO2 through Temperature Vacuum Swing Adsorption Using MIL-101(Cr)-PEI-800 and

mmen-Mg2(dobpdc) MOF Adsorbents," *Ind Eng Chem Res*, vol. 56, no. 3, pp. 750–764, Jan. 2017, doi: 10.1021/acs.iecr.6b03887.

[54] L. Joss, M. Hefti, Z. Bjelobrk, and M. Mazzotti, "On the Potential of Phase-change Adsorbents for CO2 Capture by Temperature Swing Adsorption," in *Energy Procedia*, Elsevier Ltd, 2017, pp. 2271–2278. doi: 10.1016/j.egypro.2017.03.1375.

[55] Darunte and Lalit A, "APPLICATION OF METAL ORGANIC FRAMEWORKS (MOFs) TO CAPTURING CO2 DIRECTLY FROM AIR," PhD thesis, Georgia Institute of Technology, 2018. Accessed: Mar. 25, 2018. [Online]. Available: https://smartech.gatech.edu/handle/1853/60614

[56] L. A. Darunte *et al.*, "Moving beyond Adsorption Capacity in Design of Adsorbents for CO 2 Capture from Ultradilute Feeds: Kinetics of CO 2 Adsorption in Materials with Stepped Isotherms," *Ind Eng Chem Res*, vol. 58, no. 1, pp. 366–377, Jan. 2019, doi: 10.1021/acs.iecr.8b05042.

[57] W. K. Shi *et al.*, "Temperature-vacuum swing adsorption for direct air capture by using low-grade heat," *J Clean Prod*, vol. 414, Aug. 2023, doi: 10.1016/j.jclepro.2023.137731.

[58] M. Gholami, T. R. Van Assche, and J. F. Denayer, "Temperature vacuum swing, a combined adsorption cycle for carbon capture," Mar. 01, 2023, *Elsevier Ltd*. doi: 10.1016/j.coche.2022.100891.

[59] W. Liu, Y. C. Lin, Y. Ji, J. Y. Yong, X. J. Zhang, and L. Jiang, "Thermodynamic study on two adsorption working cycles for direct air capture," *Appl Therm Eng*, vol. 214, Sep. 2022, doi: 10.1016/j.applthermaleng.2022.118920.

[60] J. Elfving, C. Bajamundi, J. Kauppinen, and T. Sainio, "Modelling of equilibrium working capacity of PSA, TSA and TVSA processes for CO2 adsorption under direct air capture conditions," *Journal of CO2 Utilization*, vol. 22, pp. 270–277, Dec. 2017, doi: 10.1016/J.JCOU.2017.10.010.

[61] R. Hughes *et al.*, "Isotherm, Kinetic, Process Modeling, and Techno-Economic Analysis of a Diamine-Appended Metal-Organic Framework for CO2Capture Using Fixed Bed Contactors," *Energy and Fuels*, vol. 35, no. 7, pp. 6040–6055, Apr. 2021, doi: 10.1021/acs.energyfuels.0c04359.

[62] J. H. Lee *et al.*, "Enhancement of CO2 binding and mechanical properties upon diamine functionalization of M2(dobpdc) metal-organic frameworks," *Chem Sci*, vol. 9, no. 23, pp. 5197–5206, 2018, doi: 10.1039/c7sc05217k.

[63] A. Sinha and M. J. Realff, "A parametric study of the techno-economics of direct CO2 air capture systems using solid adsorbents," *AIChE Journal*, vol. 65, no. 7, Jul. 2019, doi: 10.1002/aic.16607.

[64] S. M. W. Wilson, "High purity CO2 from direct air capture using a single TVSA cycle with Na-X zeolites," *Sep Purif Technol*, vol. 294, p. 121186, Aug. 2022, doi: 10.1016/J.SEPPUR.2022.121186.

[65] M. Bagheri, M. Fakhroleslam, and S. Fatemi, "Ultra-Dilute CO2 capture in an ethane treatment plant via temperature swing adsorption: Simulation-based analysis and multi-objective optimal design," *Sep Purif Technol*, vol. 356, p. 129968, Apr. 2025, doi: 10.1016/J.SEPPUR.2024.129968.

[66] J. A. Mason *et al.*, "Application of a High-Throughput Analyzer in Evaluating Solid Adsorbents for Post-Combustion Carbon Capture via Multicomponent Adsorption of CO2, N2, and H2O," *J Am Chem Soc*, vol. 137, no. 14, pp. 4787–4803, Apr. 2015, doi: 10.1021/jacs.5b00838.

[67] J. Wu, X. Zhu, Y. Chen, R. Wang, and T. Ge, "The analysis and evaluation of direct air capture adsorbents on the material characterization level," *Chemical Engineering Journal*, vol. 450, p. 137958, Dec. 2022, doi: 10.1016/J.CEJ.2022.137958.

[68] M. Ozkan, A. A. Akhavi, W. C. Coley, R. Shang, and Y. Ma, "Progress in carbon dioxide capture materials for deep decarbonization," Jan. 13, 2022, *Elsevier Inc.* doi: 10.1016/j.chempr.2021.12.013.

[69] D. Liu *et al.*, "MOF-5 composites exhibiting improved thermal conductivity," *Int J Hydrogen Energy*, vol. 37, no. 7, pp. 6109–6117, Apr. 2012, doi: 10.1016/J.IJHYDENE.2011.12.129.

[70] R. L. Siegelman *et al.*, "Controlling Cooperative CO2 Adsorption in Diamine-Appended Mg2(dobpdc) Metal-Organic Frameworks," *J Am Chem Soc*, vol. 139, no. 30, pp. 10526–10538, Aug. 2017, doi: 10.1021/jacs.7b05858.

[71] S. Farooq and D. M. Ruthven, "Basmadjian, D. An Analysis of Adiabatic Sorption of Single Solutes in Fixed Beds: Pure Thermal Wave Formation and its Practical Implications," Academic Press, 1990. [Online]. Available: https://pubs.acs.org/sharingguidelines

[72] A. Luukkonen, J. Elfving, and E. Inkeri, "Improving adsorption-based direct air capture performance through operating parameter optimization," *Chemical Engineering Journal*, vol. 471, p. 144525, Sep. 2023, doi: 10.1016/J.CEJ.2023.144525.

[73] V. Stampi-Bombelli, M. van der Spek, and M. Mazzotti, "Analysis of direct capture of CO 2 from ambient air via steam-assisted temperature–vacuum swing adsorption," *Adsorption*, vol. 26, no. 7, pp. 1183–1197, Oct. 2020, doi: 10.1007/s10450-020-00249-w.

[74] J. A. ' 'WURZBACHER, "DEVELOPMENT OF A TEMPERATURE-VACUUM SWING PROCESS FOR CO 2 CAPTURE FROM AMBIENT AIR," Doctoral dissertation, ETH Zurich, 2015. Accessed: May 26, 2015. [Online]. Available: https://www.research-collection.ethz.ch/

[75] J. D. Martell, P. J. Milner, R. L. Siegelman, and J. R. Long, "Kinetics of cooperative CO2adsorption in diamine-appended variants of the metal-organic framework Mg2(dobpdc)," *Chem Sci*, vol. 11, no. 25, pp. 6457–6471, Jul. 2020, doi: 10.1039/d0sc01087a.

[76] Lalit A. DaruntеAloysius D. OetomoKrista S. Walton*David S. Sholl*Christopher W. Jones*, "Direct Air Capture of CO2 Using Amine Functionalized MIL-101(Cr)," *ACS Sustain Chem Eng*, vol. 4, no. 10, pp. 5761–5768, 2016.

[77] B. M. Balasubramaniam, P. T. Thierry, S. Lethier, V. Pugnet, P. Llewellyn, and A. Rajendran, "Process-performance of solid sorbents for Direct Air Capture (DAC) of CO2 in optimized temperature-vacuum swing adsorption (TVSA) cycles," *Chemical Engineering Journal*, vol. 485, p. 149568, Apr. 2024, doi: 10.1016/J.CEJ.2024.149568.

[78] J. A. Wurzbacher, C. Gebald, S. Brunner, and A. Steinfeld, "Heat and mass transfer of temperature–vacuum swing desorption for CO2 capture from air," *Chemical Engineering Journal*, vol. 283, pp. 1329–1338, Jan. 2016, doi: 10.1016/J.CEJ.2015.08.035.

[79] T. M. Mcdonald, "Synthesis and Characterization of Alkylamine-Functionalized Metal-Organic Frameworks as Adsorbents for Carbon Dioxide," University of Califirnia,Berkerly, 2015. [Online]. Available: https://escholarship.org/uc/item/8ph267b9

[80] W. 'ANDREAS, V. 'THOMAS, S. 'JAN, S. 'JOHANNES, "METHOD AND ARRANGEMENT FOR SPECTRAL BROADENING OF LASER PULSES FOR NON-LINEAR PULSE COMPRESSION ," 2017

[81] T. Deschamps, M. Kanniche, L. Grandjean, and O. Authier, "Modeling of Vacuum Temperature Swing Adsorption for Direct Air Capture Using Aspen Adsorption," *Clean Technologies*, vol. 4, no. 2, pp. 258–275, Jun. 2022, doi: 10.3390/cleantechnol4020015.

[82] F. 'Olga, E. 'Christian, B. 'Mahdi, " Techno-economic assessment of CO2 direct air capture plants," *Journal of Cleaner Production* , vol. 224, pp. 957–980, 2019.

[83] S. 'Bardow, A. 'Deutz, "Life-cycle assessment of an industrial direct air capture process based on temperature–vacuum swing adsorption," *Nat Energy*, vol. 6, pp. 203–213, 2021.